

# **An Interactive Shader for Natural Diffraction Gratings**

## **Bachelorarbeit**

der Philosophisch-naturwissenschaftlichen Fakultät  
der Universität Bern

vorgelegt von

Michael Single

2014

Leiter der Arbeit:  
Prof. Dr. Matthias Zwicker  
Institut für Informatik und angewandte Mathematik

## Abstract

In nature, animals exhibit structural colors because of the physical interaction of light with the nanostructures of their skin. In his pioneering work, J.Stam developed a reflectance model based on wave optics capturing the effect of diffraction from surface nanostructures. His model is dependent on an accurate estimate of the correlation function using statistical properties of the surface's height field. We propose an adaption of his BRDF model that can handle complex natural gratings directly. Furthermore, we describe a method for interactive rendering of diffraction effects due to interaction of light with biological nanostructures such as those on snake skins. Our method uses discrete height fields of natural gratings acquired by using atomic force microscopy (AFM) as an input and employs Fourier Optics to simulate far-field diffraction. Based on a Taylor Series approximation for the phase shifts at the nanoscale surface, we leverage the precomputation of the discrete Fourier Transformations involved in our model, to achieve interactive rendering speed (about 5-15 fps). We demonstrate results of our approach using surface nanostructures of two snake species, namely the *Elaphe* and the *Xenopeltis* species, when applied to a measured snake geometry. Lastly, we evaluate the quality of our method by comparing its (peak) viewing angles with maximum reflectance for a fixed incident beam with those resulting from the grating equation at different wavelengths. We conclude that our method produces accurate results for complex, natural gratings at interactive speed.

# Contents

|          |  |           |
|----------|--|-----------|
| <b>1</b> | <b>Introduction</b>  | <b>1</b>  |
| 1.1      | Motivation . . . . .   | 1         |
| 1.2      | Goals . . . . .  | 3         |
| 1.3      | Previous work . . . . .                                      | 4         |
| 1.4      | Thesis Structure . . . . .                                   | 5         |
| <b>2</b> | <b>Theoretical Background</b>                                | <b>6</b>  |
| 2.1      | Basics in Modelling Light in Computer Graphics . . . . .     | 6         |
| 2.1.1    | Radiometry . . . . .   | 6         |
| 2.1.2    | Spectral Energy . . . . .                                    | 6         |
| 2.1.3    | Spectral Power . . . . .                                     | 7         |
| 2.1.4    | Spectral Irradiance . . . . .                                | 7         |
| 2.1.5    | Spectral Radiance . . . . .                                  | 7         |
| 2.1.6    | BRDF . . . . .   | 8         |
| 2.1.7    | Wavespectrum and Colors . . . . .                            | 9         |
| 2.1.8    | Colorspace . . . . .   | 10        |
| 2.1.9    | Spectral Rendering . . . . .                                 | 12        |
| 2.1.10   | Rendering Equation . . . . .                                 | 13        |
| 2.2      | Wave Theory for Light and Diffraction . . . . .              | 14        |
| 2.2.1    | Basics in Wave Theory . . . . .                              | 14        |
| 2.2.2    | Wave Interference . . . . .                                  | 15        |
| 2.2.3    | Wave Coherence . . . . .                                     | 16        |
| 2.2.4    | Huygen's Principle . . . . .                                 | 17        |
| 2.2.5    | Waves Diffraction . . . . .                                  | 18        |
| 2.3      | Stam's BRDF formulation . . . . .                            | 19        |
| <b>3</b> | <b>Derivations</b>   | <b>23</b> |
| 3.1      | Problem Statement and Challenges . . . . .                   | 23        |
| 3.2      | Approximate a FT by a DFT . . . . .                          | 24        |
| 3.2.1    | Reproduce FT by DTFT . . . . .                               | 24        |
| 3.2.2    | Spatial Coherence and Windowing . . . . .                    | 26        |
| 3.2.3    | Reproduce DTFT by DFT . . . . .                              | 27        |
| 3.3      | Adaption of Stam's BRDF for Discrete Height Fields . . . . . | 29        |
| 3.3.1    | Reflected Radiance of Stam's BRDF . . . . .                  | 29        |
| 3.3.2    | Relative Reflectance . . . . .                               | 30        |
| 3.4      | Optimization using Taylor Series . . . . .                   | 32        |
| 3.5      | Spectral Rendering using DFTs . . . . .                      | 34        |

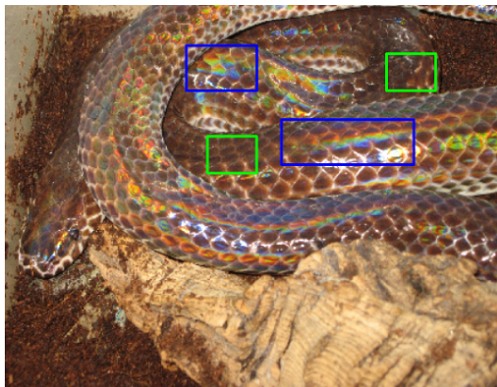
|          |  |           |
|----------|--|-----------|
| 3.6      | An Alternative Approach . . . . .                | 35        |
| 3.6.1    | PQ factors . . . . .                             | 35        |
| 3.6.2    | Sinc Interpolation in Frequency Domain . . . . . | 37        |
| <b>4</b> | <b>Evaluation and Data Acquisition</b>           | <b>39</b> |
| 4.1      | Diffraction Gratings . . . . .                   | 39        |
| 4.2      | Data Acquisition . . . . .                       | 43        |
| 4.3      | Verifications . . . . .                          | 44        |
| 4.3.1    | Numerical Comparisons . . . . .                  | 45        |
| 4.3.2    | Virtual Testbench . . . . .                      | 47        |
|          | <b>Bibliography</b>                              | <b>50</b> |

# Chapter 1

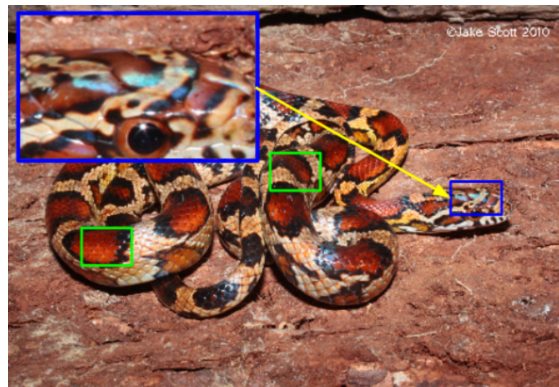
## Introduction

### 1.1 Motivation

As human beings, we visually perceive and experience our whole world in terms of colors resulting from various physical phenomena that involve interaction between light and matter. Particularly in nature, there are basically two main causes for color production. Firstly, due to pigmentation, which occurs since certain molecules in a biological structure selectively absorb or reflect specific wavelengths from an incident light source. And secondly because of structural colors, which are the result of physical interaction of light with a nanostructure, exclusively relying on the structuring of the material and not on any other property. A natural diffraction grating is a semitransparent layer of biological nano-structures that exhibits a certain degree of regularity to produce structural colors by diffracting an incident light beam. One particular example for such biological color production includes the spectacular colors that we can see while having a closer look at the illuminated skin of snakes, as shown in figure 1.1.



(a) Xenopeltis snake



(b) Elaphe Guttata snake

Figure 1.1: Examples of pigmentation color (green boxes) and structural color (blue boxes) on different snake species<sup>1</sup>.

<sup>1</sup>The image source for figure 1.1(a) is [http://www.snakes-alive.co.uk/gallery\\_5.html](http://www.snakes-alive.co.uk/gallery_5.html) and for figure 1.1(b) is [http://www.the-livingrainforest.co.uk/living/view\\_price.php?id=464](http://www.the-livingrainforest.co.uk/living/view_price.php?id=464)

Some species, like the Xenopeltis, express structural colors in form of iridescent patterns along their scales way stronger than others such as the Elaphe species. The reason lies in the nanostructure of their skins. There are a vast amount of additional reasons for structural color occurrences in nature, such as thin film interference, intra-cellular photonic crystals or diffraction gratings. More detailed examples are shown in figure 1.2.

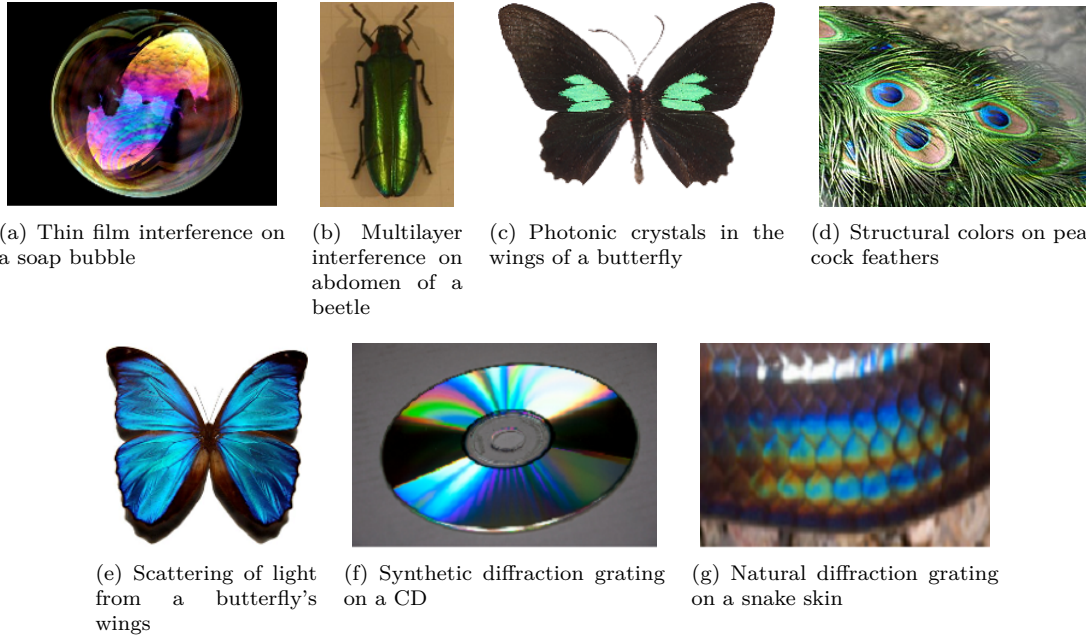


Figure 1.2: Examples<sup>2</sup> for structural colors on wings and abdomen of insects, liquids, synthetic structures, and on scales on the skin of reptiles.

As far back as in the 17th century, Robert Hooke was able to relate the cause of structural colors to the microstructure of a material. During his examinations of peacock feathers (see figure 1.2(d)), he found that by wetting the feathers, their colors disappeared. Further, he observed that the feathers have tiny ridges. Later, building on top of the knowledge about interference at this time, Newton related structural colors to wave interference. Recently, in the field of computer graphics, many researchers have developed models to render structural colors. Most of these currently available models are not able to perform interactive rendering or are oversimplified and thus cannot accurately model the effects of diffraction from natural gratings.

<sup>2</sup>image source for figures:

- 1.2(a): [http://www.ualberta.ca/~pogosyan/teaching/PHYS\\_130/FALL\\_2010/lectures/lect33/lecture33.html](http://www.ualberta.ca/~pogosyan/teaching/PHYS_130/FALL_2010/lectures/lect33/lecture33.html)
- 1.2(b): <http://www.itp.uni-hannover.de/~zawischa/ITP/multibeam.html>
- 1.2(c): [http://upload.wikimedia.org/wikipedia/commons/a/a4/Parides\\_sesostris\\_MHNT\\_dos.jpg](http://upload.wikimedia.org/wikipedia/commons/a/a4/Parides_sesostris_MHNT_dos.jpg)
- 1.2(d): [http://en.wikipedia.org/wiki/Structural\\_coloration](http://en.wikipedia.org/wiki/Structural_coloration)
- 1.2(e): From paper [MT10], figure 6.
- 1.2(f): <http://cnx.org/content/m42496/latest/?collection=col11428/latest>
- 1.2(g): [http://www.snakes-alive.co.uk/gallery\\_5.html](http://www.snakes-alive.co.uk/gallery_5.html)

This thesis investigates this particular problem in detail and provides a solution for rendering structural colors that are caused by diffraction on natural gratings at interactive rates.

## 1.2 Goals

The purpose of this thesis is, to simulate physically accurate structural colors caused by the effect of diffraction on various biological structures and then implement this simulation as a renderer with interactive behaviour. We mainly focus on structural colors generated by natural diffraction gratings. In particular the approach presented in this thesis applies to surfaces with quasiperiodic structures at the nanometer scale, which can be represented as height fields and are visualized as grayscale images<sup>3</sup>.

Natural gratings are found on the scale of reptiles, wings of butterflies or the bodies of various insects, but we restrict ourselves and focus on snake skins. The data of our discrete valued height fields, which are representing the surface of a measured snake skin, is acquired using atomic force microscopy (AFM)<sup>4</sup>. Figure 1.3 shows a measured height field of a Xenopeltis snake as a grayscale image. The surface of its skin is composed of many finger like structures. Locally, these fingers seem to be very regularly aligned (red box). However, globally, we observe that the alignment of the fingers is curved irregularly (indicated by green curves) along the whole surface. This kind of global irregularity is what makes it hard to model the structural complexity of natural gratings<sup>5</sup>.

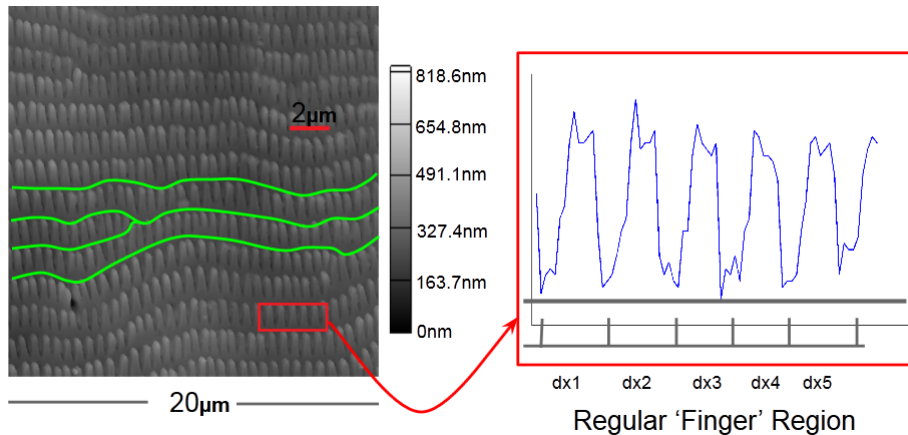


Figure 1.3: Height field of a Xenopeltis snake<sup>6</sup> skin taken using AFM. Locally, this natural grating consists of regularly aligned (red box) finger-like substructures, but globally we observe a curved alignment of these structures (green curves).

Our renderer established in this thesis is based on the pioneering work of J. Stam about diffraction shaders [Sta99]. Stam formulated a BRDF modelling the effect of diffraction based on certain sta-

<sup>3</sup>By the term *grayscale image* we are referring to a certain representation of a height field by visualizing its relative depth in a certain way. Its relative depth is color encoded by color values ranging from black (a height value of zero) to white (maximum height value of height field)

<sup>4</sup>All data is provided by the Laboratory of Artificial and Natural Evolution in Geneva. See their website: [www.lanevol.org](http://www.lanevol.org)

<sup>5</sup>E.g. by relying on statistical methods, capturing surface details by introducing an appropriate distribution function of the finger structures.

<sup>6</sup>This image was provided by the LANE lab in Geneva

tistical properties of height fields. Nevertheless we have to adapt his BRDF model, since his model assumes that a given surface of a grating can either be formulated by an analytical function and therefore has a closed form solution, or it is modelled effectively by relying on statistical methods. However, we are dealing with natural diffraction gratings (represented as explicitly formulated height fields), which unfortunately are neither known analytically, nor do they fit into simple statistical models. This thesis thus proposes an extension to J. Stam's work for the complex case of explicitly defined, discrete and quasi-periodic height field structures.

In the following section a brief overview of relevant previous work and related to this thesis will be presented.

### 1.3 Previous work

The first scientific descriptions of structural colors were provided by Hooke in 1665 in his book Micrographia[R.H12]. Hooke investigated feathers of peacocks using one of the first microscopes from his time and found out that the colors on the feather were canceled out whenever a drop of water moistened the feather. He proposed the speculation that a layer of thin plates and air were responsible for reflecting the light and thus he related the structure of the feather to colors. In Newton's book Opticks[I.N14] he described that the colors of the peacock feather are related to the thinness of the transparent part of the feathers. Around 1800, T. Young demonstrated wave interference using his double-slit experiment<sup>7</sup>[T.Y07]. In his work Young explained light as a result of wave interference. He also related structural colors to the concept of wave interference. He published his findings in the journal Philosophical Transactions of the Royal Society.

In the field of computer graphics, J.Stam[Sta99] developed a popular reflection model that could produce colorful diffraction effects, based on certain statistical properties of a given height field. His model is an approximation of far field diffraction<sup>8</sup> effects relying on the Kirchhoff integral<sup>9</sup>. For a certain class of surfaces which can be modelled as a height field he provides an analytical solution of the BRDF model. He assumes homogeneity of the structure and the main idea of his paper is to formulate the BRDF as a function of the Fourier Transform of certain correlation functions relating to the given height field. However, the height fields that Stam is dealing with are either extremely regular or can be considered as a superposition of randomly distributed bumps forming a periodic like structure relying on probabilistic distribution theory<sup>10</sup>. Either of assumptions allow him to derive an analytical solution using statistical models. However, the height field we are dealing with are measured, complex, biological nano-structures and thus they do not exhibit regularity at a global scale as demonstrated in figure 1.3. Superimposing one particular nano finger (considering it as a bump) cannot capture the complexity of the measured structure since this structure is globally highly irregular aligned. Thus, using only one finger poses a non-trivial problem of modelling the distribution of nano fingers statistically. Therefore, we cannot directly use Stam's BRDF model when we want to enable interactive rendering for diffraction effects of natural gratings.

In 2012 Cuypers et all [CT12] proposed a wave based Bidirectional scattering distribution function (BSDF<sup>11</sup>) denoted as WBSDF. Using the rendering equation and Wigner Distribution

---

<sup>7</sup>See [http://en.wikipedia.org/wiki/Double-slit\\_experiment](http://en.wikipedia.org/wiki/Double-slit_experiment)

<sup>8</sup>See [http://en.wikipedia.org/wiki/Fraunhofer\\_diffraction](http://en.wikipedia.org/wiki/Fraunhofer_diffraction)

<sup>9</sup>See [http://en.wikipedia.org/wiki/Kirchhoff\\_integral\\_theorem](http://en.wikipedia.org/wiki/Kirchhoff_integral_theorem)

<sup>10</sup>See [http://en.wikipedia.org/wiki/Probability\\_distribution](http://en.wikipedia.org/wiki/Probability_distribution)

<sup>11</sup>See [http://en.wikipedia.org/wiki/Bidirectional\\_scattering\\_distribution\\_function](http://en.wikipedia.org/wiki/Bidirectional_scattering_distribution_function)

Functions<sup>12</sup> (WDF) they related their WBSDF model to the incoming wavefront and hence, their model can be adapted such that it can be rendered by a Monte Carlo renderer. The advantage of their model over Stam's is that their models also captures near field diffraction effects. A disadvantage of their model is that it is computational expensive since the WDF of a two dimensional surface is a four dimensional function and therefore can hardly be used in order to perform interactive rendering.

Linday and Agu [CT12] proposed an approach in order to perform interactive rendering diffraction effect by precomputing and storing their BRDF model using spherical harmonics. Nonetheless, for complex natural gratings their BRDF may be insufficient accurate since their approach is using low order spherical harmonics.

## 1.4 Thesis Structure

The reminder of this thesis is organised as follows: Due to the fact that this thesis has a rather advanced mathematical complexity, chapter 2 introduces some important definitions about modelling light in computer graphics and some wave theory. These concept are required in order to be able to follow our later derivations. This is followed by a brief summary of J. Stam's Paper about diffraction shaders, since his BRDF formulation is the basis of our derivations.

In chapter 3 we adapt Stam's BRDF model step-wise in a way that we derive a representation which can be implemented as an interactive diffraction renderer for natural diffraction gratings. We also propose an alternative formulation, which we refer to as the PQ approach in this chapter and discuss its short-comings.

Chapter 4 addresses the practical part of this thesis, the implementation of our diffraction model, explaining all precomputation steps and how rendering is preformed in our reference framework for this thesis.

Chapter 5 deals with the evaluation of our models. It first provides some insights about diffraction gratings. Then, within this chapter we evaluate the qualitative validity of our BRDF model when applied on different surface gratings by computing their reflectance and comparing the results to the grating equation, under similar conditions.

Chapter 6 presents our rendered results, first the BRDF maps for all our gratings and shading approaches under various shading parameters and then the actual renderings on a snake skin. And finally Chapter 7 contains the conclusion of this thesis discussing what has been achieved in this thesis and the drawbacks of the proposed method. It also contains a note about some of my personal experiences during this thesis.

---

<sup>12</sup>See [http://en.wikipedia.org/wiki/Wigner\\_distribution\\_function](http://en.wikipedia.org/wiki/Wigner_distribution_function)

# Chapter 2

## Theoretical Background

### 2.1 Basics in Modelling Light in Computer Graphics

#### 2.1.1 Radiometry

One purpose of Computer Graphics is to simulate the interaction of light with a surface and how a real-world observer, such as a human eye, will perceive this. These visual sensations of an eye are modelled relying on a virtual camera which captures the emitted light from the surface. The physical basis to measure such reflected light is studied under radiometry which deals with measures on the electromagnetic radiation transferred from a source to a receiver.

Fundamentally, light is a form of energy propagation, consisting of a large collection of photons, whereat each photon can be considered as a quantum of light that has a position, a direction of propagation and a wavelength  $\lambda$ . A photon travels at a certain speed  $v = c/n$ , that depends only the speed of light  $c$  and the refractive index  $n$  through which it propagates. Its frequency is defined by  $f = v/\lambda$  and its carried amount of energy  $q$ , measured in the SI unit Joule, is given by  $q = hf = h\nu/\lambda n$  where  $h$  is the Plank's constant. The total energy of a large collection of photons is hence  $Q = \sum_i q_i$ .

#### 2.1.2 Spectral Energy

It is important to understand that the human eye is not equally sensitive to all wavelength of the spectrum of light and therefore responds differently to specific wavelengths. Remember that our goal is to model the human visual perception. This is why we consider the energy distribution of a light spectrum rather than considering the total energy of a photon collection since then we could weight the distribution according to the human visual system. So the question we want to answer is: How is the energy distributed across wavelengths of light?

One idea is to make an energy histogram from a given photon collection. For this we have to order all photons by their associated wavelength, discretize the wavelength spectrum, count all photons which then will fall in same wavelength-interval, and then, finally, normalize each interval by the total energy  $Q$ . This will give us a histogram which tells us the spectral energy  $Q_\lambda$  for a given discrete  $\lambda$  interval and thus models the so called spectral energy distribution<sup>1</sup>.

---

<sup>1</sup>Intensive quantities can be thought of as density functions that tell the density of an extensive quantity at an infinitesimal by a small interval or a point.

### 2.1.3 Spectral Power

Rendering an image in Computer Graphics corresponds to capturing the color sensation of an illuminated, target scene at a certain point in time. Each color is associated with either a particular wavelength or is composed of a wavelength spectrum<sup>2</sup>. Thus a color is directly related to a certain amount of energy. In order to determine the color of a to-be-rendered pixel of an image, we have to first get a sense of how much light (in terms of energy) passes through the area which the pixel corresponds to. We begin by considering the flow of energy  $\Phi = \frac{\Delta Q}{\Delta t}$  transferred through this area over a unit period of time. This allows us to measure the energy flow through a pixel during a certain amount of time. In general, power is the estimated rate of energy production for light sources and corresponds to the flux. It is measured in the unit Watts, denoted by  $Q$ . Since power is a rate over time, it is well defined even when energy production is varying over time. As with Spectral Energy for rendering, we are really interested in the spectral power  $\Phi_\lambda = \frac{\Delta \Phi}{\Delta \lambda}$ , measured in Watts per nanometer.

### 2.1.4 Spectral Irradiance

Before we can tell how much light is reflected from a given point on a surface towards the viewing direction of an observer, we first have to know how much light arrives at this point. Since in general a point has no length, area or even volume associated, let us instead consider an infinitesimal area  $\Delta A$  around a such a point. Then, we can ask ourself how much light falls in such a small area. Further while observing this process over a short period of time, the measured quantity gives us the the spectral irradiance  $E$  as illustrated in figure 2.1. Summarized, this quantity tells us how much spectral power is incident on a surface per unit area and mathematically is equal:

$$E_\lambda = \frac{\Phi_\lambda}{\Delta A} \quad (2.1)$$

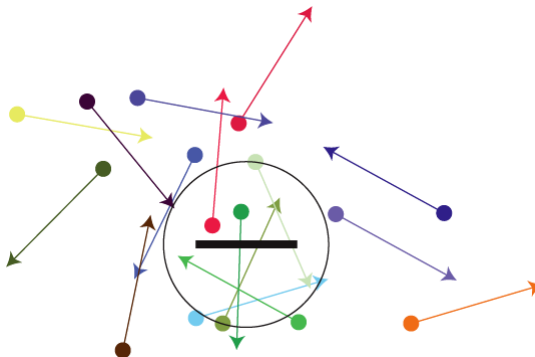


Figure 2.1: Irradiance is the summed up radiance over all directions. The black border is representing a surface element.

### 2.1.5 Spectral Radiance

When rendering an image we have to determine the color of each pixel of the image. Although irradiance tells us how much light is arriving at a point and gets reflected, it tells us nothing

---

<sup>2</sup>A wavelength spectrum is a collection of certain wavelengths. For example brown color is a composition of many wavelengths in the region of yellow, orange or read color in combination with low luminance.

about the power distribution across different directions. The direction of the element is important because the human eye may perceive the brightness of an illuminated objects differently when looking from direction.

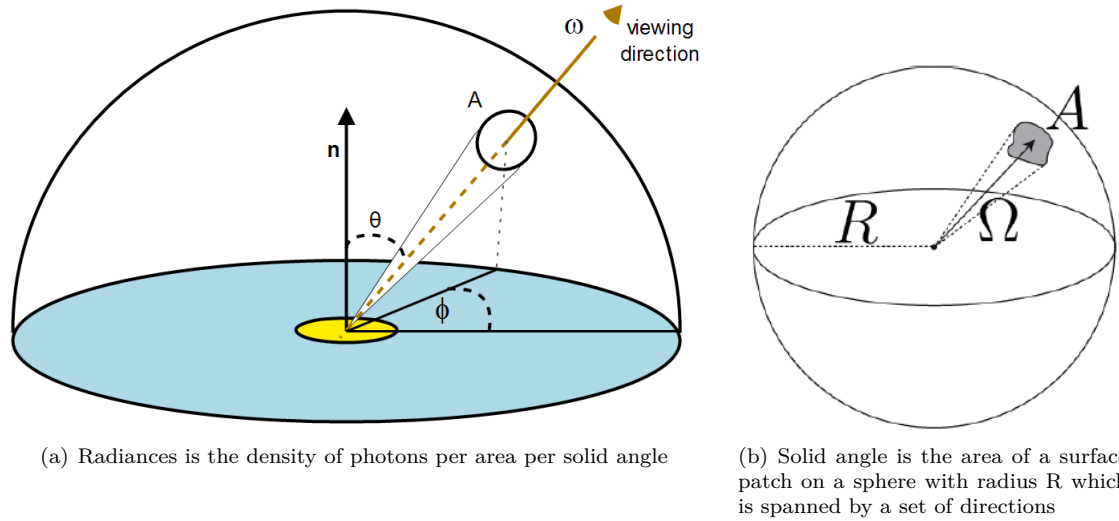


Figure 2.2: Illustration of the concepts of radiance and of solid angle and how they are related.

This concept is described by the radiometric quantity radiance. Basically, radiance is the measure of light energy passing through or emitted from a small area around a point on a surface towards a given direction during a short period in time. More formally this is the spectral power emerging from an arbitrary point (an infinitesimal area around this point) and falls within a given solid angle (see figure<sup>3</sup> 2.2(b)) in a specific direction (usually towards the observer) as shown in figure 2.2(a). Formally, this leads us to the following mathematical formalism:

$$L_\lambda(\omega) = \frac{d^2\Phi_\lambda}{dAd\Omega} \approx \frac{\Phi_\lambda}{\Omega A} \quad (2.2)$$

where  $L$  is the observed spectral radiance in  $\text{Wm}^{-2}\text{sr}^{-1}$  in direction  $\omega$ <sup>4</sup>,  $\Phi_\lambda$  is the total power emitted,  $\theta$  is the angle between the surface normal and the specified direction,  $A$  is the area of the surface and  $\Omega$  is the solid angle subtended by the observation or measurement.

It is useful to distinguish between radiance incident at a point on a surface and excitant from that point. Terms for these concepts sometimes used in the graphics literature are surface radiance  $L_r$  for the radiance *reflected* from a surface and field radiance  $L_i$  for the radiance *incident* at a surface.

### 2.1.6 BRDF

In order to render the colorization of an observed object, a natural question in Computer Graphics is what portion of the incident light a viewer will receive after reflection, after when he looks at an illuminated object. For any given surface which is illuminated from a certain direction  $\omega_i$ ,

<sup>3</sup>Modified from a figure in Computer Graphics class 2012 in chapter *Colors*

<sup>4</sup>The direction  $\omega$  is determined by two angles,  $\phi$  and  $\theta$  like illustrated in figure 2.2

we can ask ourselves how much light is reflected from any point on this surface towards a viewing direction  $\omega_r$ . This is where the Bidirectional Reflectance Distribution Function (BRDF) comes into play, which is a radiometric quantity telling us how much light is reflected at an opaque surface. Mathematically speaking, the BRDF is the ratio of the reflected radiance pointing in the direction  $\omega_r$  to the incident irradiance coming from the inverse direction of  $\omega_i$  as illustrated in figure 2.3. Hence the BRDF is a four dimensional function defined by four angles  $\theta_i$ ,  $\phi_i$ ,  $\theta_r$  and  $\phi_r$ .

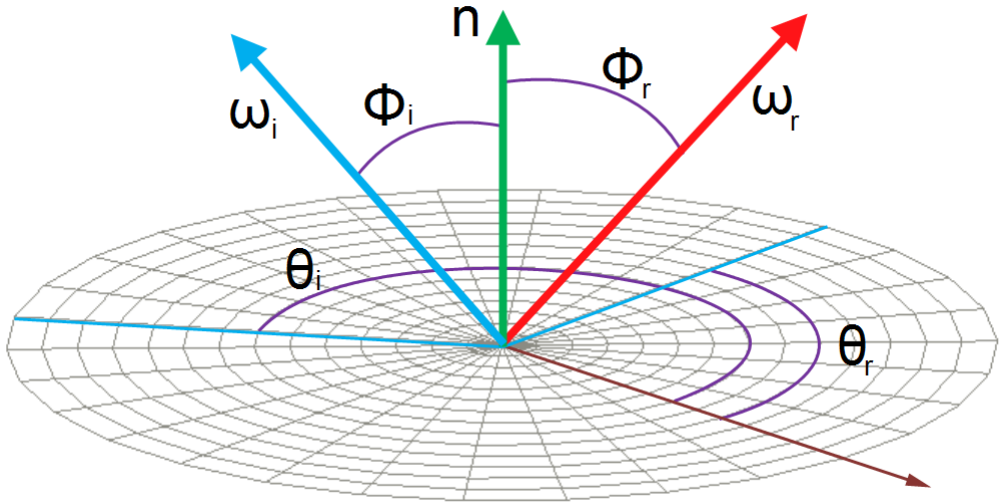


Figure 2.3: Illustration of the BRDF model, where  $\omega_i$  is pointing to the light source and the viewing direction is denoted by  $\omega_r$ . Both unit direction vectors are defined w.r.t to a surface normal  $\mathbf{n}$  for every point on the surface.

Formally, a BRDF for any given wavelength  $\lambda$  is defined as:

$$\begin{aligned} BRDF_\lambda(\omega_i, \omega_r) &= \frac{dL_r(\omega_r)}{dE_i(\omega_i)} \\ &= \frac{dL_r(\omega_r)}{L_i(\omega_i)\cos(\theta_i)d\omega_i} \end{aligned} \quad (2.3)$$

Where  $L_r$  is the reflected spectral radiance,  $E_i$  is the incident spectral irradiance and  $\theta_i$  is the angle between  $\omega_i$  and the surface normal  $\mathbf{n}$ . Also,  $L_i$  is the incident spectral radiance.

### 2.1.7 Wavespectrum and Colors

In order to see how crucial the role of human vision plays, let us consider the following definition of color by *Wyszeckiu and Siles* mentioned in the Fundamentals of Computergraphics Book[PS09], stating that "*Color is the aspect of visual perception by which an observer may distinguish differences between two structure-free fields of view of the same size and shape such as may be caused by differences in the spectral composition of the radiant energy concerned in the observation*". Therefore, similarly like the humans' perceived sensation of smell and taste, color vision is just another individual sense of perception giving us the ability to distinguish between different frequency distributions of light which we experienced as different colors.

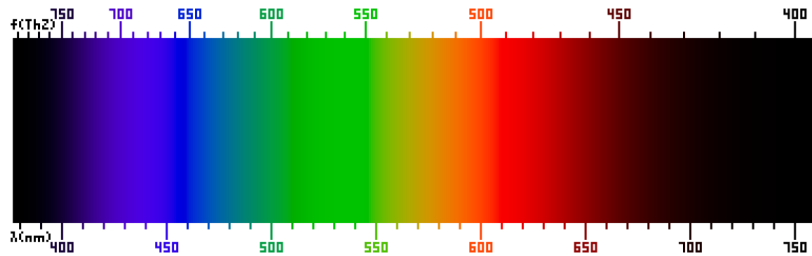


Figure 2.4: Frequency (top) and wavelength (bottom) of colors of the visible light spectrum<sup>5</sup>.

In general, an eye consists of photoreceptor cells which are responsible for providing ability of color perception. A schematic of an eye is illustrated in figure 2.5. Basically, there are two specialized types of photoreceptor cells, cone cells which are responsible for color vision and rod cells, which allow an eye to perceive different brightness levels.

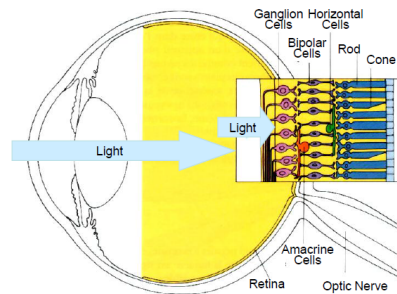


Figure 2.5: Schematic<sup>6</sup> of photoreceptor cells, cones and rods, in a human eye

A human eye is made of three different types of cone cells, having their peak sensitivity in different wavelength ranges. More precisely, there are cone cells most sensitive to short wavelengths between  $420\text{nm}$  and  $440\text{nm}$ , those which are most sensitive in the middle range between  $530\text{nm}$  and  $550\text{nm}$  and those which have their peak in the long range, from  $560\text{nm}$  to  $580\text{nm}$ . Therefore, any color sensation in human color perception can therefore be described by just three parameters, corresponding to the levels of stimulus of these three types of cone cells.

### 2.1.8 Colorspace

In order to render accurate images of how a human observer sees its world, a mathematical model of the human color perception is required. Remember that color sensation is due to a visual stimulus processed by cone cells in an eye. A human eye contains three different types of cone cells. Therefore, one possible approach is to describe each kind of these cone cells with a function mapping each wavelength to a certain sensitivity. In the early 1920 from a series of experiments, the so called CIE RGB color space was derived (see figure 2.6). This space describes the response of cone cells of an average human individual, the so called standard observer. Basically, a statistically sufficiently large number of probands were exposed to different target light colors expressed by their wavelength. The task of each proband was to reproduce these target colors by mixing

<sup>5</sup>Similar figure like used in computer graphics class 2012 in chapter colors

<sup>6</sup>image of illustration has been taken from

[http://en.wikipedia.org/wiki/Bidirectional\\_reflectance\\_distribution\\_function](http://en.wikipedia.org/wiki/Bidirectional_reflectance_distribution_function)

three given primary colors, red, green and blue light. The strength of each primary color could be manually adjusted by setting their relative sensitivity. Those adjustment weights have been measured, aggregated and averaged among all probands for each primary color. This model describes each color as a triple of three real valued numbers<sup>7</sup>, the so called tristimulus values. Summarized, these experiments provided certain weights of primary colors in order to match a color at a certain wavelength according to the average human color perception. However, some of these weights could have a negative value.

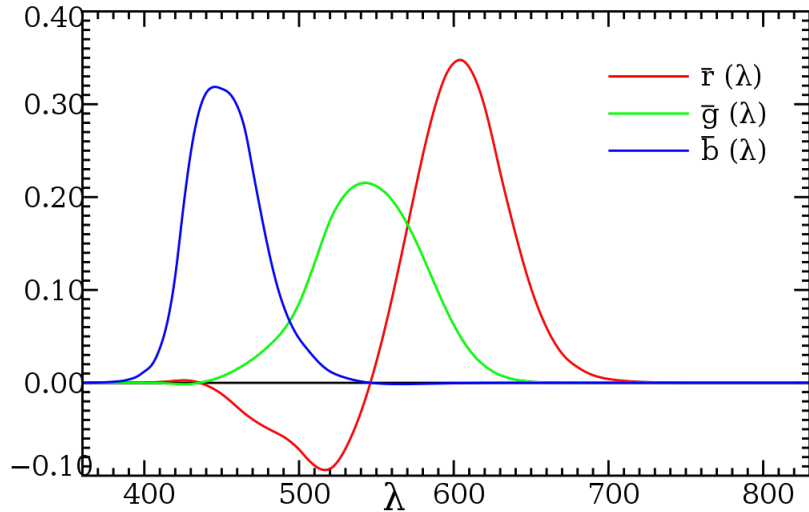


Figure 2.6: Plots<sup>8</sup> of CIE 1931 RGB Color matching functions showing the amounts of primaries needed to match a certain wavelength.

The disadvantage of the CIE RGB colorspace is that some of its color weights are negative. Thus, scientist derived the CIE XYZ colorspace which as no negative color matching functions but is still additive<sup>9</sup>. Figure 2.7 visualizes the matching functions of the CIE XYZ space. Another property of the CIE XYZ space is that its Y component is representing the luminance of the corresponding color. Usually, the CIE XYZ space is used as a reference colorspace to define colorspace transformations.

Pragmatically speaking, color spaces describe the range of colors a camera can see, a printer can print or a monitor can display. Thus, formally we can define it as a mapping from a range of physically produced colors from mixed light to a standard objective description of color sensations registered in the eye of an observer in terms of tristimulus values.

<sup>7</sup>note that there are negative color weights possible in the CIE RGB colors space. This is why some human perceived color sensations could not be reconstructed using just an additive color model (adding three positively weighted primary values). Therefore, a proband was also allowed to move one of the primary colors to the target color and instead was supposed to reproduce this new color mix using the two remaining primaries (subtractive model). The value of the selected, moved primary was then interpreted as being negative weighted in an additive color model.

<sup>8</sup>These plots have been taken from [http://en.wikipedia.org/wiki/CIE\\_1931\\_color\\_space](http://en.wikipedia.org/wiki/CIE_1931_color_space)

<sup>9</sup>Remember, the property of an additive colorspace is that any color can be represented as a weighted sum of matching functions of that color space.

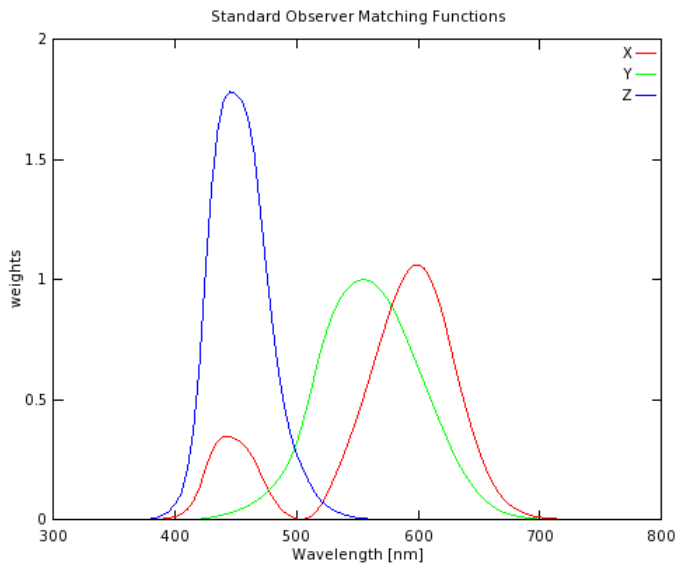


Figure 2.7: Plots of our CIE XYZ color matching functions we used for rendering

Interpolating all measured tristimuli values gives us three basis functions, the CIE color matching functions  $\bar{x}(\lambda)$ ,  $\bar{y}(\lambda)$ ,  $\bar{z}(\lambda)$ . In figure 2.7 are the numerical description of the chromatic response of the observer. They can be thought of as the spectral sensitivity curves of three linear light detectors yielding the CIE tristimulus values X, Y and Z.

The tristimulus values for a color with a spectral power distribution  $I(\lambda)$ , are given in terms of the standard observer by:

$$\begin{aligned} X &= \int_{\Lambda} I(\lambda) \bar{x}(\lambda) d\lambda \\ Y &= \int_{\Lambda} I(\lambda) \bar{y}(\lambda) d\lambda \\ Z &= \int_{\Lambda} I(\lambda) \bar{z}(\lambda) d\lambda \end{aligned} \quad (2.4)$$

where  $\lambda$  is the wavelength of the equivalent monochromatic light spectrum  $\Lambda = [380\text{nm}, 780\text{nm}]$ . Note that it is not possible to build a display that corresponds to the CIE XYZ colorspace. For this reason it is necessary to design other color spaces, which are physically realizable, efficiently encoded, perceptually uniform and have an intuitive color specification. There are simple conversions between XYZ color spaces to other color space - such as the RGB colorspace - described as linear transformations.

### 2.1.9 Spectral Rendering

When rendering an image, most of the time we are using colors described in a certain RGB color space. However, a RGB colorspace results from a colorspace transformation of the tristimulus values, which themselves are inherent to the human visual system. Therefore, many physical phenomenon are poorly modelled when they rely on RGB colors for rendering. Using only RGB colors for rendering is like assuming that a given light source emits light of only three particular

wavelengths. But in reality this is rarely the case. Spectral rendering refers to using certain wavelength spectrum, for e.g. the human visible light spectrum, instead of simply using only the range of RGB values in order to render an illuminated scene. This captures the physical reality of specific light sources way more accurately. Keep in mind that even when we make use of a spectral rendering approach, we have to convert the final spectra to RGB color values when we want to display an image on an actual display.

### 2.1.10 Rendering Equation

As discussed previously, colors are associated to radiance. Since we are starting with Stam's BRDF<sup>10</sup> formulation but want to perform a simulation rendering structural colors, we have to reformulate this BRDF equation such that we will end up with an identity of the reflected spectral radiance. This is where the rendering equation comes into play. Let us assume we are given an incoming light source directional at a solid angle  $\omega_i$  and  $\theta_i$  is its angle of incidence and that  $\omega_r$  is the solid angle for the viewing direction. Further let  $\lambda$  denote the wavelength<sup>11</sup> and  $\Omega$  is the hemisphere of integration for the incoming light. Then, we are able to formulate a  $BRDF_\lambda$  by using its definition 2.3:

$$\begin{aligned}
 f_r(\omega_i, \omega_r) &= \frac{dL_r(\omega_r)}{L_i(\omega_i)\cos(\theta_i)d\omega_i} \\
 \Rightarrow f_r(\omega_i, \omega_r)L_i(\omega_i)\cos(\theta_i)d\omega_i &= dL_r(\omega_r) \\
 \Rightarrow \int_{\Omega} f_r(\omega_i, \omega_r)L_i(\omega_i)\cos(\theta_i)d\omega_i &= \int_{\Omega} dL_r(\omega_r) \\
 L_r(\omega_r) &\implies \int_{\Omega} f_r(\omega_i, \omega_r)L_i(\omega_i)\cos(\theta_i)d\omega_i
 \end{aligned} \tag{2.5}$$

The last equation is the so called rendering equation . We assume that our incident light is a directional, unpolarized light source like sunlight and therefore its radiance is given as

$$L_\lambda(\omega) = I(\lambda)\delta(\omega - \omega_i) \tag{2.6}$$

where  $I(\lambda)$  is the intensity of the relative spectral power for the wavelength  $\lambda$ . By plugging the identity in equation 2.6 into our current rendering equation 2.5, we will get:

$$\begin{aligned}
 L_\lambda(\omega_r) &= \int_{\Omega} BRDF_\lambda(\omega_i, \omega_r)L_\lambda(\omega_i)\cos(\theta_i)d\omega_i \\
 &= BRDF_\lambda(\omega_i, \omega_r)I(\lambda)\cos(\theta_i)
 \end{aligned} \tag{2.7}$$

where  $L_\lambda(\omega_i)$  is the incident radiance and  $L_\lambda(\omega_r)$  is the radiance reflected by the given surface. Note that the integral in equation 2.7 vanishes since  $\delta(\omega - \omega_i)$  is only equal one if and only if  $\omega = \omega_i$ .

---

<sup>10</sup>Remember that a BRDF is the portion of a incident light source reflected off a given surface towards a specified viewing direction.

<sup>11</sup>Notice that, to keep our terms simple, we have dropped all  $\lambda$  subscripts for spectral radiance quantities.

## 2.2 Wave Theory for Light and Diffraction

### 2.2.1 Basics in Wave Theory

In order to prepare the reader for relevant concepts in physics which are used later for derivations and reasonings within this thesis, I am going to provide a quick introduction to the basics of wave theory and related concepts. In physics, a wave describes a disturbance that travels from one location to another through a certain medium. The disturbance temporarily displaces the particles in the medium from their rest position which results in an energy transport along the medium during wave propagation. Usually, when talking about waves we are actually referring to a complex valued function which is a solution to the so called *wave equation* which is modelling how the wave disturbance proceeds in space during time.

There are two types of waves, (a) mechanical waves which deform their mediums during propagation like sound waves and (b) electromagnetic waves consisting of periodic oscillations of an electromagnetic field, such as light. As illustrated in figure 2.8, there are several properties someone can use and apply in order to compare and distinguish different waves:

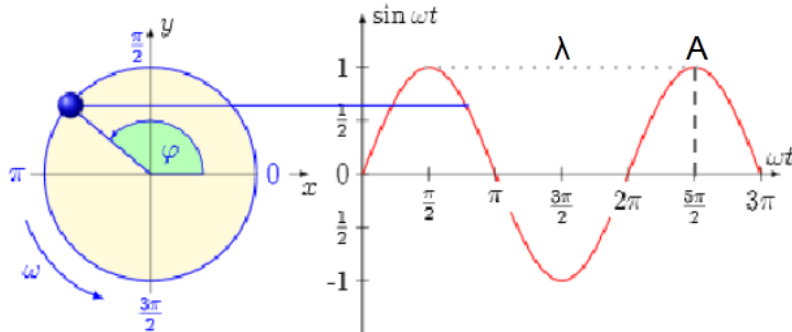


Figure 2.8: Simplified, one dimensionally real valued wave function<sup>12</sup>, giving an idea about some important wave properties. We denote the crest of a wave as the highest point relative to the equilibrium line (zero height along time axis) and similarly the trough as the lowest point.

**Wavelength:** It is usually denoted by  $\lambda$  and is a measure for the spatial distance from one point to another until the shape of a wave repeats

**Amplitude:** It is denoted by  $A$  and there are two possible interpretations: Firstly, it is a measure of the height from the equilibrium point to the highest point of a crest on the wave or the lowest point of a trough. This means that the amplitude can be positive or negative. However, usually, someone is just interested in the absolute value of an amplitude, i.e. the magnitude of a wave. For light waves it is a relative measure of intensity or brightness to other light waves of the same wavelength. And secondly, it can be interpreted as a measure how much energy a wave carries whereat the greater the absolute amplitude value, the bigger the amount of energy being carried.

**Frequency:** Is a measure of the number of waves which are passing through a particular point in the propagation medium during one unit of time and is denoted by  $f$ .

<sup>12</sup>Image source: <http://neutrino.ethz.ch/Vorlesung/FS2013/index.php/vorlesungsskript>

**Phase:** It is denoted by  $\varphi$ . It describes either the offset of initial position of a wave or the relative displacement between or among waves having the same frequency. Two waves with same frequency are said to be *in phase* if they have the same phase. This means that they line up everywhere. On the other hand, two waves are said to be *out of phase* if they have the same frequency but a different phases. As a remark, we denote by  $\omega$  the angular frequency which is equal  $2\pi f$ .

A geometrical property of waves is their wavefront. This is either a surface or line along the path of wave propagation on which the disturbance at every point has the same phase. Basically, a wavefront can have any kind of shape although three prominent types of wavefronts are: spherical-, cylindrical- and plane wavefronts. If a point in an isotropic medium is sending out waves in three dimensions, then the corresponding wavefronts are spheres, centered on the source point. Hence spherical wavefront is the result of a spherical wave, also denoted as a wavelet. Note that for electromagnetic waves, the phase is a position of a point in time on a wavefront cycle (motion of wave over a whole wavelength) whereat a complete cycle is defined as being equal to  $360^\circ$ .

### 2.2.2 Wave Interference

Next, after having seen that a wave is simply a traveling disturbance along a medium, having some special properties, someone could ask what happens when there are several waves traveling on the same medium. Especially, we are interested in how these waves will interact with each other. In physics the term interference denotes the interaction of waves when they encounter each other at a point along their propagation medium. At each point where two waves superpose, their total displacement is the sum of the displacements of each individual wave at that point. Then, the resulting wave is having a greater or lower amplitude than each separate wave and we can interpret the interference as the addition operates on waves. Two extreme scenarios are illustrated in figure 2.9 for waves with same frequency and equal amplitude. There are basically three variants of interferences which can occur, depending on how crest and troughs of the waves are matched up:

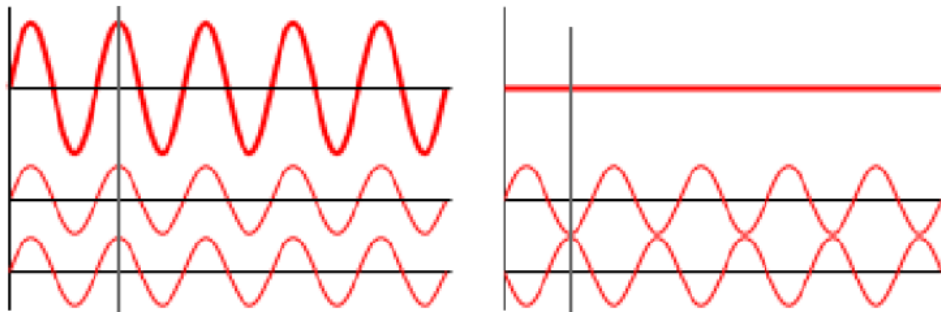


Figure 2.9: Interference scenarios<sup>13</sup> when two waves meet: On the left hand-side, there is constructive interference and on the right hand-side there is destructive interference illustrated.

- A crest of a wave meets a crest of another wave and similarly a trough meets a trough of another wave. This scenario is denoted as constructive interference and occurs at any location along the medium where the two interfering waves have a displacement in the same

<sup>13</sup>Image source: [http://en.wikipedia.org/wiki/Interference\\_\(wave\\_propagation\)](http://en.wikipedia.org/wiki/Interference_(wave_propagation))

direction. This is like saying that the phase difference between the waves is a multiple of  $2\pi$ . Then the resulting amplitude at that point is being much larger than the amplitude of an individual wave. For two waves with an equal amplitude interfering constructively, the resulting amplitude is twice as large as the amplitude of an individual wave.

- A crest of a wave meets a trough of another wave and vice versa. This scenario is denoted as destructive interference and occurs at any location along the medium where the two interfering waves have a displacement in the opposite direction. This is like saying that the phase difference between the waves is an odd multiple of  $\pi$ . Then the waves completely cancel each other out at any point they superimpose.
- If the phase difference between two waves is intermediate between the first two scenarios, then the magnitude of the displacement lies between the minimal and maximal values which we could get from constructive interference.

Keep in mind that when two or more waves interfere with each other, the resulting wave may have a different frequency. This means that interfering waves, coming from two light sources with a certain color, may produce a light of another color than they have.

### 2.2.3 Wave Coherence

When considering waves which are traveling on a shared medium along the same direction, we could examine how their phase difference is changing over time. Formulating the change in their relative phase as a function of time will provide us a quantitative measure of the synchronization between those two waves, the so called wave coherence. In order to better understand this concept, let us consider a perfectly mathematical sine wave and a second wave which is a phase-shifted replica of the first one. A property of these mathematical waves is that they keep their shape over an infinity amount of time (i.e. propagated wavelengths). In our scenario, both waves are traveling along the same direction on the same medium, as illustrated in figure 2.10.

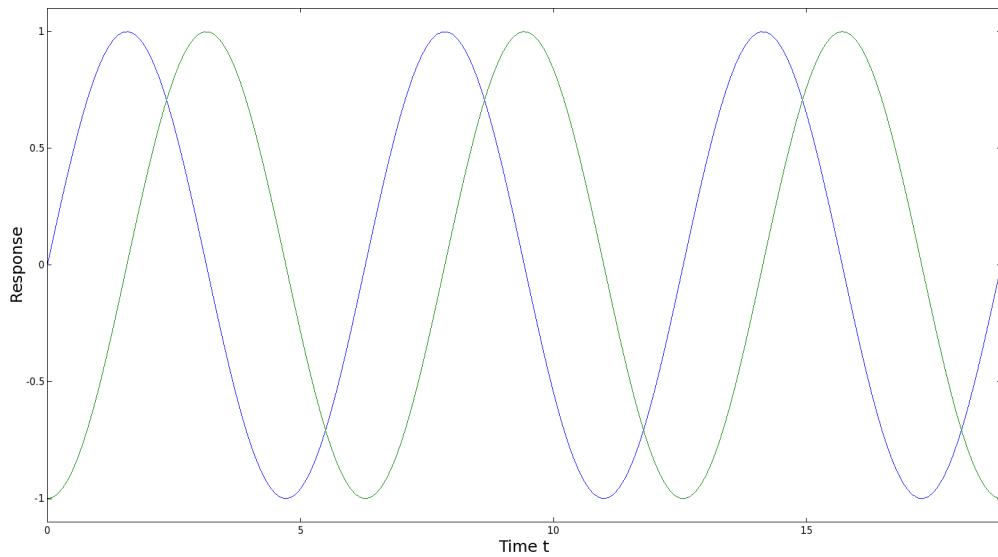


Figure 2.10: Two mathematical sine waves which are perfectly coherent which means that their phase difference is constant for every point in time.

Taking the difference between these two sine waves always yields a constant number. Therefore, those two waves are said to be coherent and hence perfectly synchronous over time. Notice that this scenario is completely artificial since in nature there are no mathematical sine waves. Rather, the phase difference is then a function of time  $p(t)$ . The more coherent two waves are, the slower this function will change over time. In fact, two waves are said to be coherent if they are of the same frequency, are temporally in phase or have the same amplitude at every point in time. Thus two waves are coherent if they are generated at the same time, having the same frequency, amplitude, and phase. Conversely, waves are considered incoherent or also asynchronous if they have no stable phase difference. This means  $p(t)$  is heavily varying over time. Coherence describes the effect of whether waves will tend to interfere with each other constructively or destructively at a certain point in time and space. Thus this is a property of waves that enables stationary interference. The more correlated two waves are, the higher their degree of coherence is. In physics coherence between waves is quantified by the cross-correlation function, which basically predicts the value of a second wave using the value of the first one. There are two basic coherence classifications:

- Spatial coherence is dealing with the question of what is the range of distance between two points in space in the span of a wave for which there is occurring a significant effect of stationary interference when averaged over time. This is formally answered by considering the correlation between waves at different point in space. The range of distance with significant coherence is also denoted as the coherence area.
- Temporal coherence examines how well two waves which are observed at two different moments in time correlate with each other. Thus it may be used for predicting how well a wave interferes temporally with itself. Mathematically, this kind of coherence is computed by measuring the correlation between the value of the wave and the delayed version of itself. The coherence time denotes the maximum time delay for which the waves are coherent. The distance a wave has traveled during the coherence time is denoted as their temporal coherence length.

#### 2.2.4 Huygen's Principle

Besides the phases and the amplitudes of waves, their propagation directly affects the interaction between different waves and how they could interfere with each other. This is why it makes sense to formulate a model which allows us to predict the position of a moving wavefront and how it moves in space. This is where *Huygen's Principle* comes into play. It states that any point of a wavefront may be regarded as a point source that emits spherical wavelets in every direction. Within the same propagation medium, these wavelets travel at the same speed as their source wavefront. The position of the new wavefront results by superimposing all of these emitted wavelets. Geometrically, the surface that is tangential to the secondary waves can be used in order to determine the future position of the wavefront. Therefore, the new wavefront encloses all emitted wavelets. Figure 2.11 visualizes Huygen's principle for a wavefront reflected off from a plane surface.

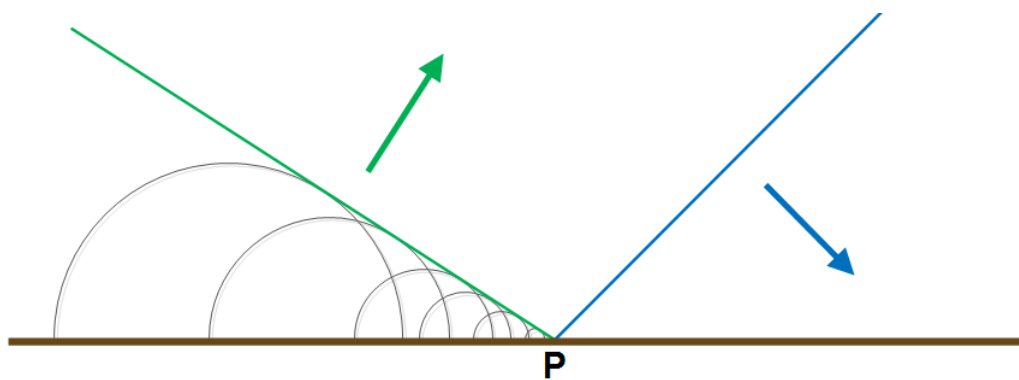


Figure 2.11: A moving wavefront (blue) encounters an obstacle (a surface shown in brown colors) and produces a new wavefront (green) as a result of superposition of all secondary wavelets.

### 2.2.5 Waves Diffraction

Revisiting Huygen's principle we know that each point on a wavefront can be considered as a source of a spherical wavelet which propagates in every direction. But what exactly happens when a wave's propagation direction is only partially occluded by an object? What will be the outcome on applying Huygen's principle to this case? An example scenario for this case is shown in figure 2.12.

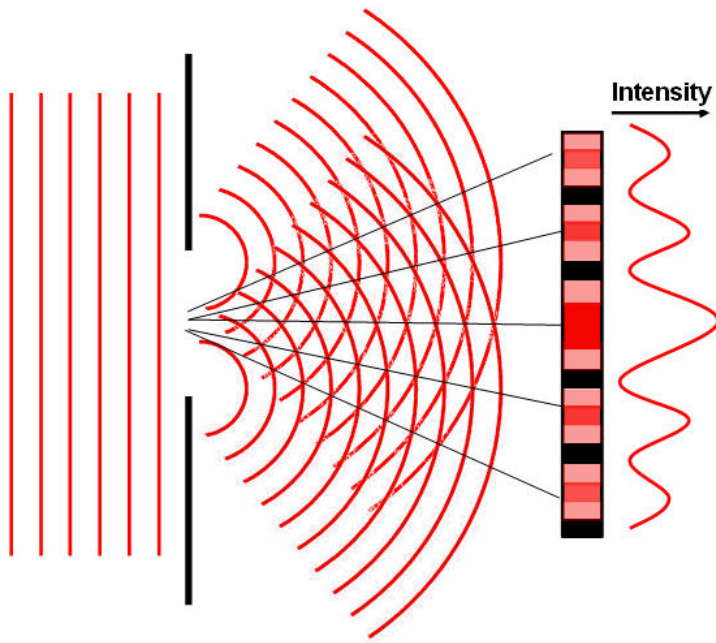


Figure 2.12: Illustration<sup>14</sup> of a diffraction scenario in which a plane wavefront passes through a surface with a certain width and how the wave will be bent, also showing the intensity of the resulting wave along a straight line in its path.

Whenever a propagating wavefront is partially occluded by an obstacle, the wave is not only moving in the direction along its propagation, but is also bent around the edges of the obstacle. In physics, this phenomenon is called diffraction. Waves are diffracted due to interference which occurs among all wavelets when applying Huygen's Principle for the case when a wavefront hits an obstacle. Generally, the effect of diffraction is most pronounced for the waves whose wavelength is roughly similar in size to the dimension of the occluding object. Conversely, if the wavelength is much smaller in size, then there is almost no wave diffraction perceivable at a far off distance. This relationship between the strength of wave diffraction and the wavelength is conceptually illustrated in figure 2.13 when a wave is transmitted through an opening in a surface. A reflective example for diffraction provided in figure 2.11.

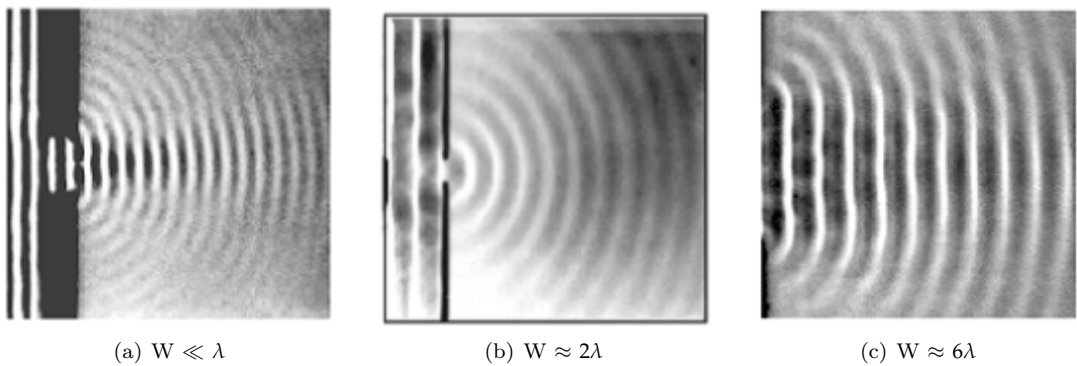


Figure 2.13: Illustration<sup>15</sup> of how diffraction changes when a wave with wavelength  $\lambda$  propagates through a slit of width equal  $W$ .

In everyday's life, we can see the direct outcome of the effect of wave diffraction in form of structural colors. There are examples from nature such as the iridescent colors on various snake skins as well as artificial examples such as the colorful patterns notable when having a close look at an illuminated compact disc. All these examples comprise a surface made of highly regular nanostructures which diffract an incident light significantly. Such a nanostructure which exhibits a certain degree of regularity is also denoted as a diffraction grating. Further information about diffraction gratings can be found in section 4.1.

## 2.3 Stam's BRDF formulation

The theoretical foundation of this thesis is based on the pioneering work of J.Stam[Sta99]. In this model Stam derived a BRDF formulation to model the effect of far field diffraction for various analytical anisotropic surfaces. His model is relying on the so called scalar wave theory of diffraction for which a wave<sup>16</sup> is assumed to be a complex valued scalar. Thus, Stam's BRDF formulation does not take into account the polarization of the incident light. Fortunately, light sources like

<sup>14</sup>Image source:[http://cronodon.com/images/Single\\_slit\\_diffraction\\_2b.jpg](http://cronodon.com/images/Single_slit_diffraction_2b.jpg)

<sup>15</sup>Image taken from:<http://neutrino.ethz.ch/Vorlesung/FS2013/index.php/vorlesungsskript>, chapter 9, figure 9.14

<sup>16</sup>In general, a wave is a complex valued vector satisfying Maxwell's equations. A scalar values wave only satisfies the Helmholtz equation. For further information please visit [http://en.wikipedia.org/wiki/Maxwells\\_equations](http://en.wikipedia.org/wiki/Maxwells_equations) and [http://en.wikipedia.org/wiki/Helmholtz\\_equation](http://en.wikipedia.org/wiki/Helmholtz_equation).

sunlight and light bulbs are unpolarized. The principal behind J. Stam's approach is illustrated in figure 2.14.

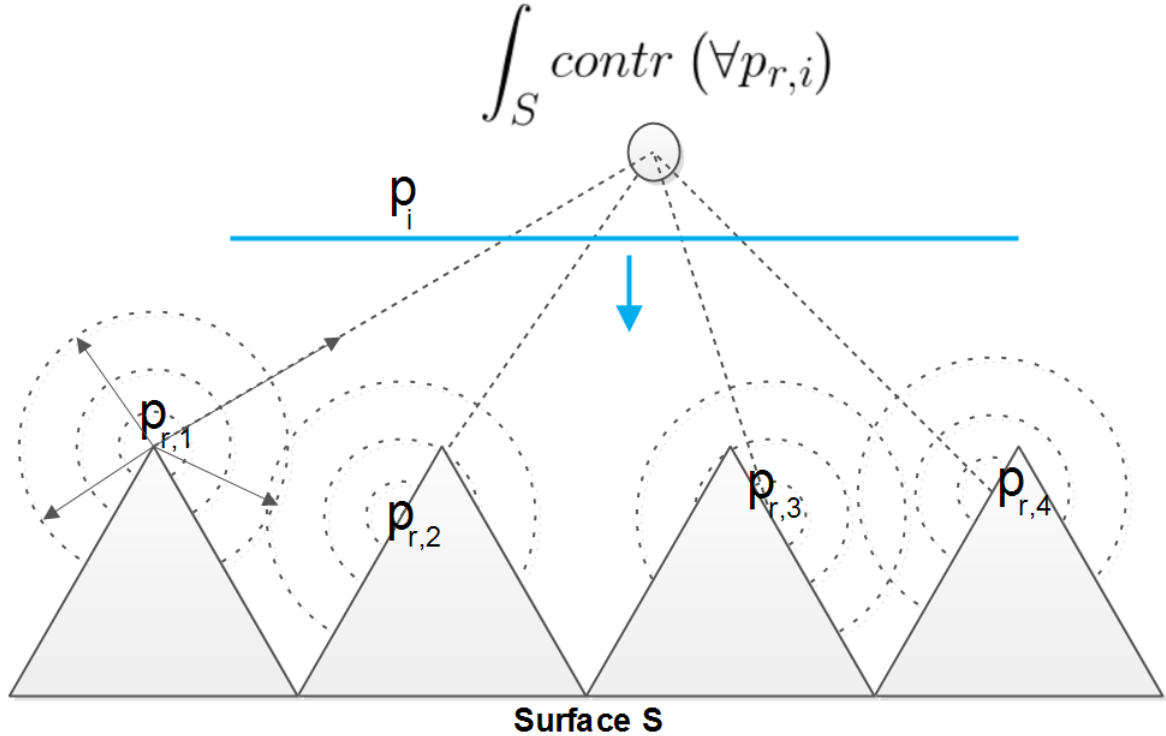


Figure 2.14: Illustration of secondary wavelets reflected off a surface. An integration over all secondary sources resulting from an incident wave according to Huygen's principle will give us an identity for the total contribution at a certain point in space.

An incident wave  $p_i$  from a light source encounters a surface representing a diffraction grating. According to Huygen's Principle, at any point  $i$  on the grating at which the incident wave meets the grating a secondary, spherical wavelet  $p_{r,i}$  will be emitted. A viewer, indicated by a gray circle in the figure, will perceive the superimposed contribution of all wavelets along the surface  $S$  (in the figure indicated by an integration symbol), which will directly follow the laws of wave interference. Therefore the resulting color which an observer sees is the final radiance at that point which reflects from stationary interference of all emitted secondary wavelets and per due to Huygen's principle.

A further assumption in Stam's Paper is, that the emanated waves from the source are stationary, which implies the wave is a superposition of independent monochromatic waves. This further implies that each wave is associated with a definite wavelength  $\lambda$ . Directional light sources such as sunlight fulfills this fact and since we are using these kinds of light sources for our simulations, Stam's model can be used for our modelling purposes.

The main idea of his model is to formulate a BRDF as a function of the Fourier transformation applied on a certain correlation function relating to the given height field. His model assumes homogeneity of the height field structure and depicts an approximation of far-field diffraction

effects. The geometrical setup of his model is illustrated in figure 2.15. The classes of surfaces his model is able to support either exhibit a very regular structure or may be considered as a superposition of bumps forming a periodic like structure. Therefore, the surfaces he is dealing with can either be modelled by probabilistic distributions or have a direct analytical representation. Both cases allow him to derive an analytical solution for his BRDF model.

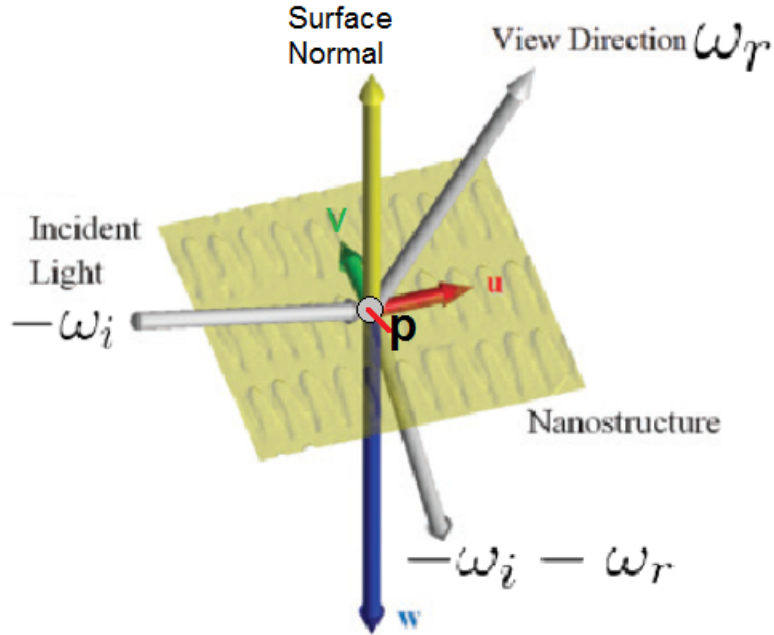


Figure 2.15: Illustration<sup>17</sup> of the geometrical setup of Stam's approach where  $\omega_i$  is a direction, pointing towards the light source,  $\omega_r$  points towards the viewer,  $n$  is the surface normal and  $(u, v, w)$  are the components of the vector  $-\omega_i - \omega_r$ .

Figure 2.15 illustrated schematically the geometrical setup used for Stam's BRDF formulation. An incident light with a direction  $\omega_i$  hits the surface of a given height field at the position  $p$ . The direction vector  $\omega_r$  points towards the viewer. After the incident light has hit the surface, a spherical wavelet is reflected off from this hit position. The direction vector of the wavelet can be computed by taking the difference between the incident and viewing direction as shown in equation 2.8:

$$(u, v, w) = -\omega_i - \omega_r \quad (2.8)$$

These coordinates will later be used in order to compute the total contribution of all secondary sources used in Stam's BRDF in equation 2.11. In Stam's Derivation, the phase difference between the incident and emitted wave from the given height field is denoted by the auxiliary function  $\Phi$  defined as in equation 2.9.

$$\Phi(x, y) = \frac{2\pi}{\lambda} wh(x, y) \quad (2.9)$$

<sup>17</sup>Modified image which originally has been taken from D.S. Dhillon et. al. poster[DD14].

Then, any secondary wavelet  $p$  which is emitted off from the given surface is equal to:

$$p(x, y) = e^{i\Phi(x, y)} \quad (2.10)$$

using the idea presented for figure 2.14 and performing all mathematical steps shown in the appendix ??, will lead us to the final BRDF representation, modelling the total contribution of all secondary sources reflected off the the provided surface  $h$  in the direction  $\omega_r$ :

$$BRDF_\lambda(\omega_i, \omega_r) = \frac{k^2 F^2 G}{4\pi^2 A w^2} \langle |P(ku, kv)|^2 \rangle \quad (2.11)$$

where  $F$  denotes the Fresnel coefficient and  $G$  is the so called geometry term<sup>18</sup> which is equal to:

$$G = \frac{(1 + \omega_i \cdot \omega_r)^2}{\cos(\theta_i) \cos(\theta_r)} \quad (2.12)$$

### Fourier Transformation Sign Convention

One last word about the Fourier transform terms that Stam uses in his derivation. Conventionally, following the definitions of the Fourier transformation, we are dealing with is commonly denoted as the inverse Fourier Transformation. However, especially in electrical engineering (EE), it is common to define the inverse Fourier transformation by the Fourier Transformation and vice versa. To be more precisely there are two definitions of the Fourier transformation. One commonly used by physicist where the exponential function is w.r.t.  $-i$  and the one which is used in EE, performing an integration over an exponential is w.r.t.  $i$ . Further information about the sign convention in Fourier transformations can be looked up in the book Quantum Mechanics for Electrical Engineers[DM12]. Note that by substituting the minus sign of the physicist definition of the Fourier transformation gives us the definition used in EE shown in in equation 2.13:

$$\begin{aligned} \mathcal{F}_{FT}\{f\}(w) &= \int_{\mathbb{R}^n} f(x) e^{-iwt} dt \\ &= \int_{\mathbb{R}^n} f(x) e^{i\hat{w}t} dt \\ &= \mathcal{F}_{FT}^{-1}\{f\}(\hat{w}) \end{aligned} \quad (2.13)$$

where  $\hat{w}$  is equal  $-w$ .

The height fields we are dealing with in this work are, however, natural gratings containing a complex shaped nano-structure and hence far from being very regularly aligned. The reason why Stam's approach in its current form is not suitable for our purpose is twofold: First his approach does not capture the complexity of natural gratings accurately well enough when relying on his statistical approaches and secondly it is way too slow in order to be usable for interactive rendering since his BRDF needs an evaluation of a Fourier Transform for every directional changing.

---

<sup>18</sup>The geometric terms expresses the correction factor to perform an integration over an area instead over a surface. For further information, please have a look at [http://en.wikipedia.org/wiki/Surface\\_integral](http://en.wikipedia.org/wiki/Surface_integral), and read the definition about *surface element*

# Chapter 3

## Derivations

### 3.1 Problem Statement and Challenges

The goal of this thesis is to perform a physically accurate and interactive simulation of structural color production as shown in figure 3.2, which we can see whenever light is diffracted from a natural grating. For this purpose we need the following input data (see figure 3.1):

- A mesh representing a snake surface<sup>1</sup> as shown in figure 3.1(a).
- A natural diffraction grating represented as a height field, its maximum height and its pixel width<sup>2</sup>.
- A vector field which describes how the given nanostructure patch is oriented on the surface (see figure 3.1(c)).

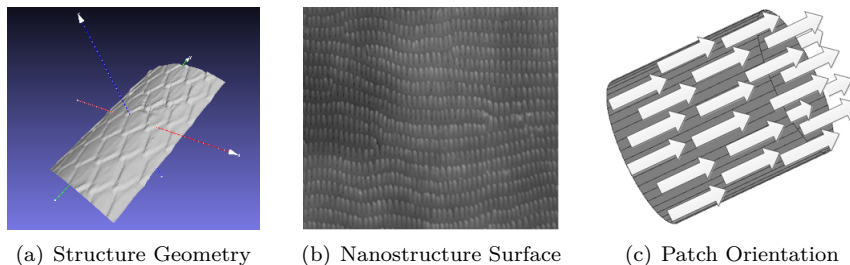


Figure 3.1: Input for our simulation

We want to rely on the integral equation 2.11 derived by J. Stam in his paper [Sta99] about diffraction shaders. This equation formulates a BRDF modelling the effect of diffraction under the assumption that a given grating can either be formulated as an analytical function or its structure is simple enough being modelled relying on statistical methods. These assumptions guarantee that 2.11 has an explicit solution. However, the complexity of a biological nanostructure cannot

<sup>1</sup>In our simulation it is an actual reconstruction of a real snake skin. These measurements are provided by the Laboratory of Artificial and Natural Evolution at Geneva. See their website: [www.lanevol.org](http://www.lanevol.org).

<sup>2</sup>Since the nanostructure is stored as a grayscale image, we need a scale telling us what length and height one pixel corresponds to in this provided image.

sufficiently and accurately modelled simply using statistical methods. This is why interactive computation at high resolution becomes a hard task, since we cannot evaluate the given integral equation on the fly. Therefore, we have to adapt Stam's equation such that we are able to perform interactive rendering using explicitly provided height fields at interactive rates.

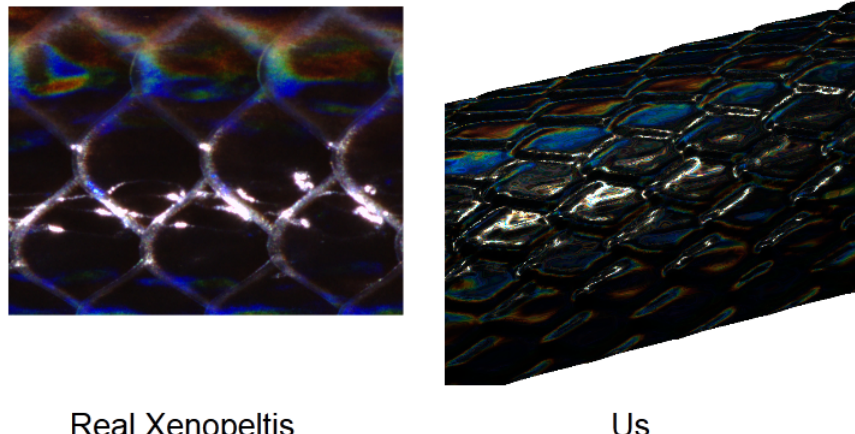


Figure 3.2: Output: Rendered Structural Colors

## 3.2 Approximate a FT by a DFT

### 3.2.1 Reproduce FT by DTFT

In the previous section, we have found an identity for the reflected spectral radiance  $L_\lambda(\omega_r)$  when using Stam's BRDF for a given input height field. However, the derived expression in equation 3.10 requires to evaluate the Fourier Transform of our height field<sup>3</sup> for every direction. In this section we explain how to approximate the FT by the DTFT and apply it to our previous derivations. Figure 3.3 graphically shows how to obtain the DTFT from the FT for a one dimensional signal<sup>4</sup>

The first step is to uniformly discretize the given signal since computers are working finite, discrete arithmetic. We rely on the Nyquist–Shannon sampling theorem tells us how dense we have to sample a given signal  $s(x)$  such that can be reconstructed its sampled version  $\hat{s}[n]$ <sup>5</sup>. In particular, a sampled version according to the Nyquist–Shannon sampling theorem will have the same Fourier transform as its original signal when it has a limited bandwidth. The sampling theorem states that if  $f_{max}$  denotes the highest frequency of  $s(x)$ , then, it has to be sampled by a rate of  $f_s$  with  $2f_{max} \leq f_s$  in order to be reconstructable. By convention  $T = \frac{1}{f_s}$  represent the interval length between two samples.

<sup>3</sup>actually it requires the computation of the inverse Fourier Transform of a transformed version of the given height field, the function  $p(x,y)$  defined in equation 2.10.

<sup>4</sup>For our case we are dealing with a two dimensional, spatial signal, the given height field. Nevertheless, without any constraints of generality, the explained approach applies to multi dimensional problems.

<sup>5</sup>Images of function plots taken from [http://en.wikipedia.org/wiki/Discrete\\_Fourier\\_transform](http://en.wikipedia.org/wiki/Discrete_Fourier_transform) and are modified.

<sup>6</sup> $n$  denotes the number of samples.

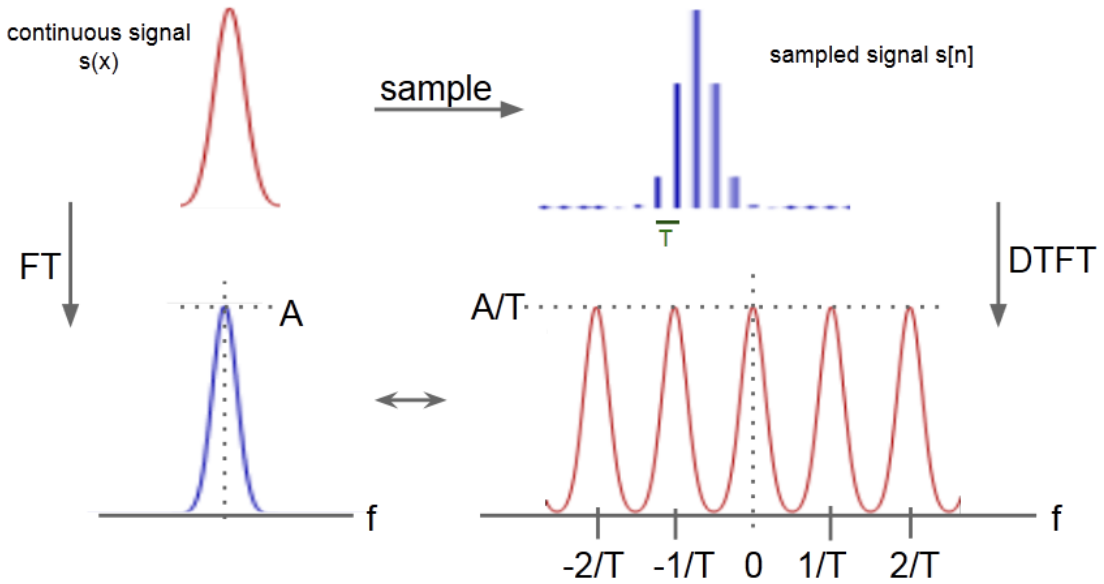


Figure 3.3: Illustration of how to approximate the analytical Fourier Transform (FT)<sup>5</sup> of a given continuous signal by a Discrete Time Fourier Transform (DTFT). The DTFT applied on a band-limited, discretized signal yields a continuous, periodic response in frequency space.

Next, we apply the Fourier transformation operator on the discretized signal  $\hat{s}$  which gives us the following expression:

$$\begin{aligned}
 \mathcal{F}_{FT}\{\hat{s}\}(w) &= \int_{\mathbb{R}} \hat{s}[n] e^{-iwx} dx \\
 &= \int_{\mathbb{R}} \text{mask}(x) s(x) e^{-iwx} dx \\
 &= T \sum_{x=-\infty}^{\infty} \hat{s}[x] e^{-iwx} \\
 &= T \mathcal{F}_{DTFT}\{s\}(w)
 \end{aligned} \tag{3.1}$$

Equation 3.1 tells us that if  $\hat{s}$  is sufficiently sampled, then its DTFT corresponds to the FT of  $s(x)$ . Notice that the resulting DTFT from the sampled signal has a height of  $\frac{A}{T}$  where  $A$  is the height of the FT of  $s$  and thus is a scaled version of the FT.

For a given height field  $h$ , let us compute Stam's auxiliary function  $p$  defined as in equation 2.10. For the remainder of this thesis we introduce the following definition:

$$P_{dtft} \equiv \mathcal{F}_{DTFT}\{p\} \tag{3.2}$$

Therefore  $P_{dtft}$  denotes the DTFT of a transformed version of our height field  $h$ <sup>7</sup>.

<sup>7</sup>By transformed height field we mean  $p(x, y) = e^{i\frac{2\pi}{\lambda} wh(x, y)}$  which we get, when we plug  $h$  into equation 2.9 and this expression again plug into equation 2.10.

### 3.2.2 Spatial Coherence and Windowing

Before we can derive a final expression in order to approximate a FT by a DFT, we first have to revisit the concept of coherence introduced in section 2.2.3 of chapter 2. Previously we have seen that wave-theory tells us what is the total contribution of all secondary sources which allows us to say what is the reflected spectral radiance at a certain point in space. This is related to stationary interference which itself depends on the coherence property of the emitted secondary wave sources. The ability for two points in space,  $t_1$  and  $t_2$ , to interfere in the extend of a wave when being averages over time is the so called spatial coherence. The spatial distance between such two points over which there is significant interference is limited by the quantity coherence area. For filtered sunlight on earth this is equal to  $65\mu\text{m}$ <sup>8</sup>.

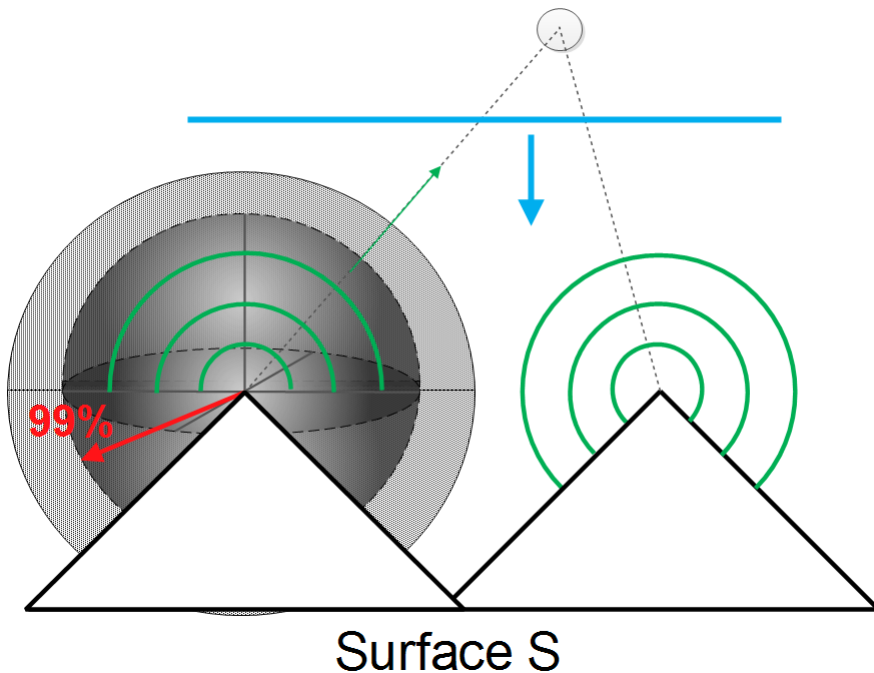


Figure 3.4: A plane wave encounters a surface. According to Huygens principle, secondary wavelets are emitted off from this surface. The resulting wave at a certain point in space (here indicated by a gray circle) depends on the interference among all waves encountering at this position. The amount of significant interference is directly affected by the spatial coherence property of all the wavelets.

Figure 3.4 illustrates the concept of spatial coherence. A wavefront (blue line) encounters a surface. Due to Huygen's principle, secondary wavelets are emitted off from the surface. The reflected radiance at a certain point in space, e.g. at a viewer's eye position (denoted by the gray circle), is a result of interference among all wavelets at that point. This interference is directly affected by the spatial coherence property of all the emitted wavelets.

In physics spatial coherence is predicted by the cross correlation between  $t_1$  and  $t_2$  and usually

---

<sup>8</sup>A proof for this number can be looked up in the book Optical Coherence and Quantum Optics[LM95] on page 153 and 154.

modelled by a Gaussian Random Process. For any such Gaussian Process we can use a spatial gaussian window  $g(x)$  which is equal:

$$g(x) = \frac{1}{\sqrt{2\pi} \cdot \sigma_s} \cdot e^{-\frac{x^2}{2\sigma_s^2}} \quad (3.3)$$

We have chosen standard deviation  $\sigma_s$  of the window such that it fulfills the equation  $4\sigma_s = 65\mu m$ . This is equivalent to saying that we want to predict about 99.99%<sup>9</sup> of the resulting spatial coherence interference effects in our model by a cross correlation function.

By applying the Fourier transformation to the spatial window we get the corresponding window in frequency space as:

$$G(f) = e^{-\frac{f^2}{2\sigma_f^2}} \quad (3.4)$$

Notice that this frequency space window has a standard deviation  $\sigma_f$  equal to  $\frac{1}{2\pi\sigma_s}$ . Those two windows, the spatial- and the frequency space window, will be used in the next section in order to approximate the DTFT by the DFT by a windowing approach.

### 3.2.3 Reproduce DTFT by DFT

In this section we explain how and under what assumptions the DTFT of a discretized signal<sup>10</sup> can be approximated by a DFT. The whole idea how to reproduce the DTFT by DFT is schematically illustrated in figure 3.5.

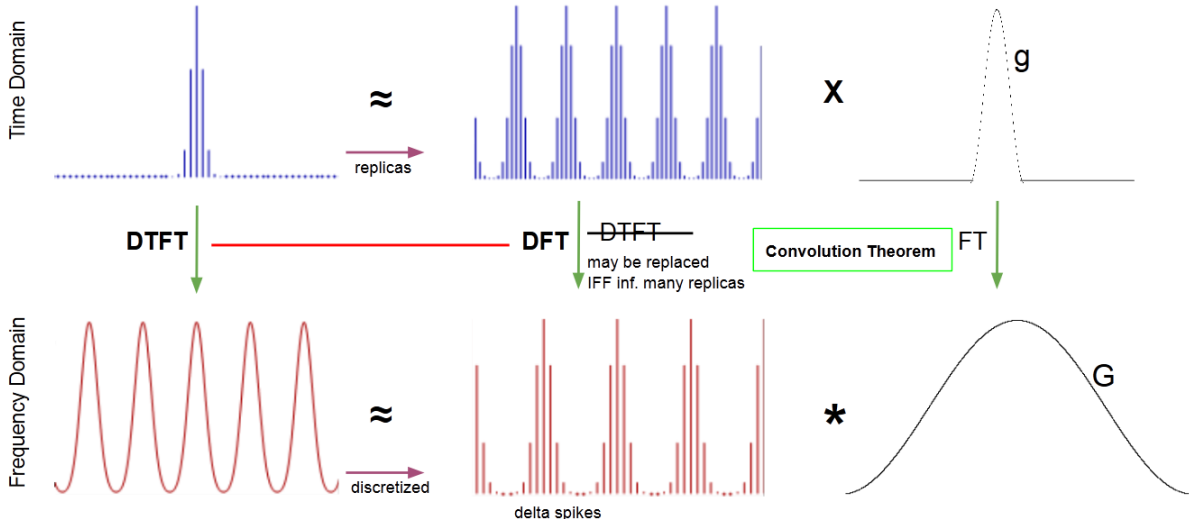


Figure 3.5: Illustration of how to approximate the DTFT<sup>11</sup> by the DFT relying on the Convolution Theorem, using a gaussian window function.

<sup>9</sup>Standard deviation values from confidence intervals table of normal distribution provided by Wolfram MathWorld <http://mathworld.wolfram.com/StandardDeviation.html>.

<sup>10</sup>E.g. a sampled signal like already presented in figure 3.3

<sup>11</sup>Images of function plots taken from [http://en.wikipedia.org/wiki/Discrete\\_Fourier\\_transform](http://en.wikipedia.org/wiki/Discrete_Fourier_transform) and are modified. Note that the scales in the graphic are not appropriate.

Lets say, we are given a spatial, band-limited and discretized one dimensional signal  $\hat{s}$ . Our goal is to approximate this spatial signal in a way such that when taking the DFT of this approximated signal, it will yield the same response as taking the DTFT of the original sampled  $\hat{s}$ . For this purpose we will use the previously introduced concept of gaussian windows and the so called Convolution Theorem which is a fundamental property of all Fourier transformations.

The Convolution Theorem states that the Fourier transformation of a product of two functions,  $f$  and  $g$ , is equal to convolving the Fourier Transformations of each individual function. Mathematically, this statement corresponds to equation 3.5:

$$\mathcal{F}\{f \cdot g\} = \mathcal{F}\{f\} * \mathcal{F}\{g\} \quad (3.5)$$

The principal issue is how to approximate our given signal  $\hat{s}$ . Therefore, let us consider another signal  $s_N^*$  which is the  $N$  times replicated version of  $\hat{s}$  (blue signal at center top in figure).

Remember that, in general, the wave magnitude at a certain point in space is the result of interference among all wavelength meeting at that position. In our scenario, the source of those signals are emitted secondary wavelets. The interference strength between wavelets is related to their spatial coherence. Windowing the signal by a gaussian window  $g$  is akin to modelling the effects of spatial coherence interference on the surface. From the previous section 3.2.2 we know that we can use gaussian window like in equation 3.3 in order to approximate such spatial signals interference effects.

Using this insight, we can approximate  $\hat{s}$  by taking the product of  $s_N^*$  with a gaussian window  $g$ . This fact is illustrated in the first row of figure 3.3. So, what will the DTFT of this approximation yield? We already know that the DTFT of  $\hat{s}$  is a continuous, periodic signal, since  $\hat{s}$  is band-limited. Thus, taking the DTFT of this found approximation should give us approximatively the same continuous, periodic signal.

This is where the convolution theorem comes into play: Applying the DTFT to the product of  $s_N^*$  and  $g$  is the same as convolving the DTFT of  $s_N^*$  by DTFT of  $g$ . From equation 3.4 we already know that the DTFT of  $g$  is just another gaussian, denoted by  $G$ . On the other hand the DTFT of  $s_N^*$  yields a continuous, periodic signal. The higher the value of  $N$ , the sharper the signal gets (denoted by delta spiked) and the closer it converges toward to the DFT. This is why the DFT is the limit of a DTFT applied on periodic and discrete signals. Therefore, for a large number of  $N$  we can replace the DTFT by the DFT operator when applied on  $s_N^*$ .

Lastly, we see that the DTFT of  $\hat{s}$  is approximately the same like convolving a gaussian window by the DFT of  $s_N^*$ . This also makes sense, since convolving a discrete, periodic signal (DFT of  $s_N^*$ ) by a continuous window function  $G$  yields a continuous, periodic function.

In general, for every non-windowed signal, we cannot compute its DTFT ?? numerically due to finite computer arithmetic and hence working with the DFT is our only option. Furthermore, there are numerically fast algorithms in order to compute the DFT values of a function, the Fast Fourier Transformation (FFT). The DFT ?? of a discrete height field is equal to the DTFT of an infinitely periodic function consisting of replicas of the same height field. Now, let a spatial gaussian window  $g$  having a standard deviation for which  $4\sigma_s$  is equal  $65\mu m$ . Then, from before, it follows:

$$\mathcal{F}_{dtft}\{\mathbf{s}\} \equiv \mathcal{F}_{dft}\{\mathbf{s}\} * G(\sigma_f) \quad (3.6)$$

Therefore we can deduce the following expression:

$$\begin{aligned}
\mathcal{F}_{dft}\{\mathbf{t}\}(u, v) &= \int_{-\infty}^{\infty} \int_{-\infty}^{\infty} F_{dft}\{\mathbf{t}\}(w_u, w_v) \phi(u - w_u, v - w_v) dw_u dw_v \\
&= \int_{-\infty}^{\infty} \int_{-\infty}^{\infty} \sum_i \sum_j F_{dft}\{\mathbf{t}\}(w_u, w_v) \\
&\quad \delta(w_u - w_i, w_v - w_j) \phi(u - w_u, v - w_v) dw_u dw_v \\
&= \sum_i \sum_j \int_{-\infty}^{\infty} \int_{-\infty}^{\infty} F_{dft}\{\mathbf{t}\}(w_u, w_v) \\
&\quad \delta(w_u - w_i, w_v - w_j) \phi(u - w_u, v - w_v) dw_u dw_v \\
&= \sum_i \sum_j F_{dft}\{\mathbf{t}\}(w_u, w_v) \phi(u - w_u, v - w_v)
\end{aligned} \tag{3.7}$$

where

$$\phi(x, y) = \pi e^{-\frac{x^2+y^2}{2\sigma_f^2}} \tag{3.8}$$

### 3.3 Adaption of Stam's BRDF for Discrete Height Fields

#### 3.3.1 Reflected Radiance of Stam's BRDF

We are going to use Stam's main derivation (2.11) for the  $BRDF(\omega_i, \omega_r)$  in 2.7 by applying the fact that the wavenumber is equal  $k = \frac{2\pi}{\lambda}$ :

$$\begin{aligned}
BRDF(\omega_i, \omega_r) &= \frac{k^2 F^2 G}{4\pi^2 A w^2} \langle |P(ku, kv)|^2 \rangle \\
&= \frac{4\pi^2 F^2 G}{4\pi^2 A \lambda^2 w^2} \langle |P(ku, kv)|^2 \rangle \\
&= \frac{F^2 G}{A \lambda^2 w^2} \left\langle \left| P\left(\frac{2\pi u}{\lambda}, \frac{2\pi v}{\lambda}\right) \right|^2 \right\rangle
\end{aligned} \tag{3.9}$$

Going back to equation 2.7 and plugging equation 3.9 into it, using the definition of equation 2.12 and the equation ?? for  $\omega$  we will get the following:

$$\begin{aligned}
L_\lambda(\omega_r) &= \frac{F^2 (1 + \omega_i \cdot \omega_r)^2}{A \lambda^2 \cos(\theta_i) \cos(\theta_r) \omega^2} \left\langle \left| P\left(\frac{2\pi u}{\lambda}, \frac{2\pi v}{\lambda}\right) \right|^2 \right\rangle \cos(\theta_i) I(\lambda) \\
&= I(\lambda) \frac{F^2 (1 + \omega_i \cdot \omega_r)^2}{\lambda^2 A \omega^2 \cos(\theta_r)} \left\langle \left| P\left(\frac{2\pi u}{\lambda}, \frac{2\pi v}{\lambda}\right) \right|^2 \right\rangle
\end{aligned} \tag{3.10}$$

Note that the Fresnel term  $F$  is actually a function of  $(w_i, w_r)$ , but in order to keep the equations simple, we omitted its arguments.

So far we just plugged Stam's BRDF identity into the rendering equation and hence have not significantly deviated from his formulation. Keep in mind that  $P$  denotes the Fourier transform

of the provided height field which depends on the viewing and incidence light direction. Thus this Fourier Transform has to be recomputed for every direction which will slow down the whole computation quite a lot<sup>12</sup>. One particular strategy to solve this issue is to approximate  $P$  by the Discrete Fourier Transform (DFT)<sup>13</sup> and separate its computation such that terms for many directions can be precomputed and then later retrieved by look ups. The approximation of  $P$  happens in two steps: First we approximate the Fourier Transform by the Discrete Time Fourier Transform (DTFT) and then, afterwards, we approximate the DTFT by the DFT. For further about basics of signal processing and Fourier Transformations please consult the appendix ??.

Using the insight gained by equation 3.1 allows us to further simplify equation 3.10:

$$\begin{aligned} L_\lambda(\omega_r) &= I(\lambda) \frac{F^2(1 + \omega_i \cdot \omega_r)^2}{\lambda^2 A w^2 \cos(\theta_r)} \left\langle \left| P\left(\frac{2\pi u}{\lambda}, \frac{2\pi v}{\lambda}\right) \right|^2 \right\rangle \\ &= I(\lambda) \frac{F^2(1 + \omega_i \cdot \omega_r)^2}{\lambda^2 A w^2 \cos(\theta_r)} \left\langle \left| T^2 P_{dtft}\left(\frac{2\pi u}{\lambda}, \frac{2\pi v}{\lambda}\right) \right|^2 \right\rangle \end{aligned} \quad (3.11)$$

Where  $P_{dtft}$  is a substitute for  $\mathcal{F}_{DTFT}\{s\}(w)$ . Furthermore  $T$  the sampling distance for the discretization of  $p(x, y)$  assuming equal and uniform sampling in both dimensions  $x$  and  $y$ .

### 3.3.2 Relative Reflectance

In this section we are going to explain how to scale our BRDF formulation such that all of its possible output values are mapped into the range  $[0, 1]$ . Such a relative reflectance formulation will ease our life for later rendering purposes since usually color values are within the range  $[0, 1]$ , too. Furthermore, this will allow us to properly blend the resulting illumination caused by diffraction with a texture map.

Let us examine what  $L_\lambda(\omega_r)$  will be for a purely specular surface, for which  $\omega_r = \omega_0 = \omega_i$  such that  $\omega_0 = (0, 0, 1)$ . For this specular reflection case, the corresponding radiance will be denoted as  $L_\lambda^{spec}(\omega_0)$ . We define the relative reflected radiance for our problem 3.10 by simply taking the fraction between  $L_\lambda(\omega_r)$  and  $L_\lambda^{spec}(\omega_0)$  which is denoted by:

$$\rho_\lambda(\omega_i, \omega_r) = \frac{L_\lambda(\omega_r)}{L_\lambda^{spec}(\omega_0)} \quad (3.12)$$

Notice that the third component  $w$  from the vector in equation 2.8 is squared equal to  $(\cos(\theta_i) + \cos(\theta_r))^2$ <sup>14</sup>. But first, let us derive the following expression:

---

<sup>12</sup>Even a fast variant of computation the Fourier Transform has a runtime complexity of  $O(N \log N)$  where  $N$  is the number of sample.

<sup>13</sup>See appendix ?? for further information about different kinds of Fourier transformations.

<sup>14</sup>Consult section ?? in the appendix

$$\begin{aligned}
L_{\lambda}^{spec}(\omega_0) &= I(\lambda) \frac{F(\omega_0, \omega_0)^2 (1 + \begin{pmatrix} 0 \\ 0 \\ 1 \end{pmatrix} \cdot \begin{pmatrix} 0 \\ 0 \\ 1 \end{pmatrix})^2}{\lambda^2 A (\cos(0) + \cos(0))^2 \cos(0)} \langle \left| T_0^2 P_{dtft}(0, 0) \right|^2 \rangle \\
&= I(\lambda) \frac{F(\omega_0, \omega_0)^2 (1+1)^2}{\lambda^2 A (1+1)^2 1} \left| T_0^2 N_{sample} \right|^2 \\
&= I(\lambda) \frac{F(\omega_0, \omega_0)^2}{\lambda^2 A} \left| T_0^2 N_{sample} \right|^2
\end{aligned} \tag{3.13}$$

Where  $N_{samples}$  is the number of samples of the DTFT  $\langle \cdot \rangle$ . Thus, we can plug our last derived expression 3.13 into the definition for the relative reflectance radiance 3.12 in the direction  $w_r$  and we get:

$$\begin{aligned}
\rho_{\lambda}(\omega_i, \omega_r) &= \frac{L_{\lambda}(\omega_r)}{L_{\lambda}^{spec}(\omega_0)} \\
&= \frac{I(\lambda) \frac{F(\omega_i, \omega_r)^2 (1 + \omega_i \cdot \omega_r)^2}{\lambda^2 A (\cos(\theta_i) + \cos(\theta_r))^2 \cos(\theta_r)} \langle \left| T_0^2 P_{dtft}(\frac{2\pi u}{\lambda}, \frac{2\pi v}{\lambda}) \right|^2 \rangle}{I(\lambda) \frac{F(\omega_0, \omega_0)^2}{\lambda^2 A} \left| T_0^2 N_{sample} \right|^2} \\
&= \frac{F^2(\omega_i, \omega_r) (1 + \omega_i \cdot \omega_r)^2}{F^2(\omega_0, \omega_0) (\cos(\theta_i) + \cos(\theta_r))^2 \cos(\theta_r)} \langle \left| \frac{P_{dtft}(\frac{2\pi u}{\lambda}, \frac{2\pi v}{\lambda})}{N_{samples}} \right|^2 \rangle
\end{aligned} \tag{3.14}$$

For simplification and better readability, let us define the following gain-factor:

$$C(\omega_i, \omega_r) = \frac{F^2(\omega_i, \omega_r) (1 + \omega_i \cdot \omega_r)^2}{F^2(\omega_0, \omega_0) (\cos(\theta_i) + \cos(\theta_r))^2 \cos(\theta_r) N_{samples}^2} \tag{3.15}$$

Using equation 3.15, we get the following expression for the relative reflectance radiance from equation 3.14:

$$\rho_{\lambda}(\omega_i, \omega_r) = C(\omega_i, \omega_r) \langle \left| P_{dtft}(\frac{2\pi u}{\lambda}, \frac{2\pi v}{\lambda}) \right|^2 \rangle \tag{3.16}$$

Using the previous definition for the relative reflectance radiance equation 3.12:

$$\rho_{\lambda}(\omega_i, \omega_r) = \frac{L_{\lambda}(\omega_r)}{L_{\lambda}^{spec}(\omega_0)}$$

which we can rearrange to the expression:

$$L_{\lambda}(\omega_r) = \rho_{\lambda}(\omega_i, \omega_r) L_{\lambda}^{spec}(\omega_0) \tag{3.17}$$

Let us choose  $L_{\lambda}^{spec}(\omega_0) = S(\lambda)$  such that it has the same profile as the relative spectral power distribution of CIE Standard Illuminant D65 (discussed in ??). Furthermore, when integrating over  $\lambda$  for a specular surface, we should get  $CIE_{XYZ}$  values corresponding to the white point for D65. The corresponding tristimulus values using CIE colormatching functions 2.4 for the  $CIE_{XYZ}$  values look like:

$$\begin{aligned} X &= \int_{\lambda} L_{\lambda}(\omega_r) \bar{x}(\lambda) d\lambda \\ Y &= \int_{\lambda} L_{\lambda}(\omega_r) \bar{y}(\lambda) d\lambda \\ Z &= \int_{\lambda} L_{\lambda}(\omega_r) \bar{z}(\lambda) d\lambda \end{aligned} \quad (3.18)$$

where  $\bar{x}$ ,  $\bar{y}$ ,  $\bar{z}$  are the color matching functions. Combining our last finding from equation 3.17 for  $L_{\lambda}(\omega_r)$  with the definition of the tristimulus values from equation 3.18, allows us to derive a formula for computing the colors values using Stam's BRDF formula relying on the rendering equation 2.5. Without any loss of generality it suffices to derive an explicit expression for just one tristimulus term, for example  $Y$ , the luminance:

$$\begin{aligned} Y &= \int_{\lambda} L_{\lambda}(\omega_r) \bar{y}(\lambda) d\lambda \\ &= \int_{\lambda} \rho_{\lambda}(\omega_i, \omega_r) L_{\lambda}^{spec}(\omega_0) \bar{y}(\lambda) d\lambda \\ &= \int_{\lambda} \rho_{\lambda}(\omega_i, \omega_r) S(\lambda) \bar{y}(\lambda) d\lambda \\ &= \int_{\lambda} C(\omega_i, \omega_r) \left\langle \left| P_{dtft} \left( \frac{2\pi u}{\lambda}, \frac{2\pi v}{\lambda} \right) \right|^2 \right\rangle S(\lambda) \bar{y}(\lambda) d\lambda \\ &= C(\omega_i, \omega_r) \int_{\lambda} \left\langle \left| P_{dtft} \left( \frac{2\pi u}{\lambda}, \frac{2\pi v}{\lambda} \right) \right|^2 \right\rangle S(\lambda) \bar{y}(\lambda) d\lambda \\ &= C(\omega_i, \omega_r) \int_{\lambda} \left\langle \left| P_{dtft} \left( \frac{2\pi u}{\lambda}, \frac{2\pi v}{\lambda} \right) \right|^2 \right\rangle S_y(\lambda) d\lambda \end{aligned} \quad (3.19)$$

Where we used the definition  $S_y(\lambda) \bar{y}(\lambda)$  in the last step.

## 3.4 Optimization using Taylor Series

Our final goal is to render structural colors resulting by the effect of wave diffraction. So far, we have derived an expression which can be used for rendering. Nevertheless, our current equation 3.19 used for computing structural colors, cannot directly be used for interactive rendering, since  $P_{dtft}$  had to be recomputed for every change in any direction<sup>15</sup>.

In this section, we will address this issue and deliver an approximation for  $P_{dtft}$  defined in equation 3.2. This approximation will allow us to separate  $P_{dtft}$  in a certain way such that some computational expensive terms can be precomputed. The main idea is to formulate  $P_{dtft}$  as a series expansion relying on the definition of Taylor Series, as defined in equation ???. Further, we will provide an error bound for our approximation approach for a given number of terms. Lastly, we will substitute our approximation into our BRDF formula from equation 3.19.

Let us consider  $p(x, y) = e^{ikwh(x, y)}$  form Stam's Paper 2.3 where  $h(x, y)$  is a given height field and  $k = \frac{2\pi}{\lambda}$  denotes the wavenumber of wavelength  $\lambda$ . For any complex number  $t$  the power series expansion of the exponential function is equal to:

---

<sup>15</sup>According to changes in viewing- or incident light direction.

$$e^t = 1 + t + \frac{t^2}{2!} + \frac{t^3}{3!} + \dots = \sum_{n=0}^{\infty} \frac{t^n}{n!} \quad (3.20)$$

Now, when we use the exponent<sup>16</sup> of  $p(x, y)$  as an input argument for equation 3.20 we get:

$$\begin{aligned} e^t &= e^{ikwh} \\ &= 1 + (ikwh) + \frac{1}{2!}(ikwh)^2 + \frac{1}{3!}(ikwh)^3 + \dots \\ &= \sum_{n=0}^{\infty} \frac{(ikwh)^n}{n!}. \end{aligned} \quad (3.21)$$

where  $i$  is the imaginary unit for complex numbers. For simplification, in the remainder of this section we omitted the arguments of  $h$ . Equation 3.21 gives us an expression for an exponential series expansion for the exponent of  $p(x, y)$ . Please note that the above Taylor series is convergent for any complex valued number. Therefore the equation 3.21 is equal to

$$p(x, y) = \sum_{n=0}^{\infty} \frac{(ikwh(x, y))^n}{n!} \quad (3.22)$$

and thus gives us a series representation of  $p(x, y)$ . Next, calculating the Fourier transformation  $\mathcal{F}$  of equation 3.22 gives us the identity:

$$\begin{aligned} \mathcal{F}\{p\} &\equiv \mathcal{F}\left\{\sum_{n=0}^{\infty} \frac{(ikwh)^n}{n!}\right\} \\ &\equiv \sum_{n=0}^{\infty} \mathcal{F}\left\{\frac{(ikwh)^n}{n!}\right\} \\ &\equiv \sum_{n=0}^{\infty} \frac{(ikw)^n}{n!} \mathcal{F}\{h^n\} \end{aligned} \quad (3.23)$$

Where we have exploited the fact that the Fourier transformation is a linear operator. Therefore, in equation 3.23, we have shown that the Fourier transformation of a series is equal to the sum of the Fourier transformation, applied on each individual series term. Reusing the identifier  $P$ <sup>17</sup> in order to determine the Fourier transformation of  $p$  from equation 2.10 equation 3.23 then correspond to:

$$P(\alpha, \beta) = \sum_{n=0}^{\infty} \frac{(ikw)^n}{n!} \mathcal{F}\{h^n\}(\alpha, \beta) \quad (3.24)$$

Up to now we have found a infinity series representation for  $P_{dtft}$ . Next we are going to look for an upper bound  $N \in \mathbb{N}$  such that

$$\tilde{P}_N(\alpha, \beta) := \sum_{n=0}^N \frac{(ikwh)^n}{n!} \mathcal{F}\{h^n\}(\alpha, \beta) \approx P(\alpha, \beta) \quad (3.25)$$

---

<sup>16</sup>This exponent is a complex valued function, equal to  $ikwh(x, y)$ .

<sup>17</sup>This identifier  $P$  may be subscripted by  $dtft$  which will denote the DTFT variant of  $P$ .

$\tilde{P}_N$  is a good approximation of  $P$ , i.e. their absolute difference is small<sup>18</sup>. But first, the following two facts would have to be proven<sup>19</sup>:

1. Show that there exist such an  $N \in \mathbb{N}$  s.t. the approximation of equation 3.25 holds true.
2. Find a value for  $N$  s.t. this approximation is below a certain error bound, e.g. close to machine precision  $\epsilon$ .

Our facts are valid and proven (see appendix ??) implies that there actually exists such an  $N$ . Thus, we can make use of the taylor series approximation from equation 3.25 and use it for approximating  $P_{dft}$ . This idea allows us to adapt equation 3.19, which is used for computing the structural colors of our BRDF model, in a numerically fast way. Finally the equation for the luminance is equal to:

$$\begin{aligned} Y &= C(w_i, w_r) \int_{\lambda} \left\langle \left| P_{dft} \left( \frac{2\pi u}{\lambda}, \frac{2\pi v}{\lambda} \right) \right|^2 \right\rangle S_y(\lambda) d\lambda \\ &= C(w_i, w_r) \int_{\lambda} \left\langle \sum_{n=0}^N \frac{(wk)^n}{n!} \mathcal{F}\{i^n h^n\} \left( \frac{2\pi u}{\lambda}, \frac{2\pi v}{\lambda} \right) \right\rangle^2 S_y(\lambda) d\lambda \end{aligned} \quad (3.26)$$

Notice that equation 3.26 is constrained by  $N$  and hence is an approximation of equation 3.19. Furthermore, it is possible to separate out all the Fourier Terms in the summation and precompute them. This is why the approach in equation 3.26 is fast in order to compute structural color values according to our BRDF model.

### 3.5 Spectral Rendering using DFTs

In this section we describe how our final model for rendering structural colors due to diffraction will look like. For this purpose we use all our previous findings and plug them together to one big equation. For a given height field  $h$  representing the surface of a grating, we want to compute the resulting color due to light diffracted on that grating. For rendering we rely on the  $CIE_{XYZ}$  colorspace. For given direction vectors  $w_i$  and  $w_r$  as shown in figure 2.15 the DFT of the height field is equal to:

$$DFT_n\{h\}(u, v) = F_{dft}\{i^n h^n\} \left( \frac{2\pi u}{\lambda}, \frac{2\pi v}{\lambda} \right) \quad (3.27)$$

From section 3.2.3 we know that we can reproduce a FT by applying a Gaussian window on the DFT from equation 3.27. This windowing approach gives us:

$$W_n(u, v) = \sum_{(r,s) \in \mathcal{N}_1(u,v)} |DFT_n\{h\}(u - w_r, v - w_s)|^2 \phi(u - w_r, v - w_s) \quad (3.28)$$

where  $\phi(x, y) = \pi e^{-\frac{x^2+y^2}{2\sigma_f^2}}$  is the Gaussian window from equation 3.2.3 and  $\mathcal{N}_1(u, v)$  denotes an the k-ring neighborhood around  $(u, v)$  with  $k$  as a parameter.

---

<sup>18</sup>Mathematically speaking, this statement correspond to  $||\tilde{P}_N - P|| \leq \epsilon$ , where  $\epsilon > 0$  is a small number.

<sup>19</sup>Please have a look in section ?? in the appendix

In section 3.4 we derived equation 3.26 which tells us how to compute the  $CIE_{XYZ}$  color value of a particular color channel using our relative reflectance BRDF model from section 3.3.2. Plugging all these findings together and using our windowing approach, listed in equation 3.28, Then  $\forall(u, v, w)$  like (defined in equation 2.8), our final expression for computing structural colors due to diffraction, using all our previous derivations, will be equal:

$$\begin{pmatrix} X \\ Y \\ Z \end{pmatrix} = C(\omega_i, \omega_r) \int_{\Lambda} \sum_{n=0}^N \frac{(2\pi w)^n}{\lambda^n n!} W_n(u, v) \begin{pmatrix} S_x(\lambda) \\ S_y(\lambda) \\ S_z(\lambda) \end{pmatrix} d\lambda \quad (3.29)$$

Where  $C(\omega_i, \omega_r)$  is the defined in equation 3.15. Note that equation 3.29 integrates over a given wavelength spectrum, denoted by  $\Lambda$ . Usually, this  $\Lambda$  is equal to  $[\lambda_{min}, \lambda_{max}]$  where  $\lambda_{min} = 380nm$  and  $\lambda_{max} = 780nm$ .

## 3.6 An Alternative Approach

### 3.6.1 PQ factors

In this section we are presenting an alternative approach to the previous Gaussian window approach described in section 3.2.3 in order to solve the issue of working with the  $DTFT$  instead of  $DFT$ . We assume, that a given surface  $S$  is covered by a number of replicas of a provided representative surface patch  $f$ . In a simplified, one dimensional scenario, mathematically speaking,  $f$  is assumed to be a repetitive function, i.e.  $\forall x \in \mathbb{R} : S(x) = S(x + nT)$ , where  $T$  is its fundamental period and  $n \in \mathbb{N}_0$ . Thus, the surfaces can be written formally as:

$$S(x) = \sum_{n=0}^N f(x + nT) \quad (3.30)$$

What we are looking for is an identity for the Fourier transform<sup>20</sup> of our surface  $S$ , required in order to simplify the  $(X, Y, Z)$  colors from 3.26:

$$\begin{aligned} \mathcal{F}\{S\}(w) &= \int f(x) e^{iwx} dx \\ &= \int_{-\infty}^{\infty} \sum_{n=0}^N f(x + nT) e^{iwx} dx \\ &= \sum_{n=0}^N \int_{-\infty}^{\infty} f(x + nT) e^{iwx} dx \end{aligned} \quad (3.31)$$

Next, apply the following substitution  $x + nT = y$  which will lead us to:

$$\begin{aligned} x &= y - nT \\ dx &= dy \end{aligned} \quad (3.32)$$

---

<sup>20</sup>Remember that we are using the definition of Fourier Transform used in electrical engineering where  $\mathcal{F}$  actually corresponds to the inverse Fourier Transform.

Plugging this substitution back into equation 3.31 we will get:

$$\begin{aligned}
\mathcal{F}\{S\}(w) &= \sum_{n=0}^N \int_{-\infty}^{\infty} f(x + nT) e^{iwx} dx \\
&= \sum_{n=0}^N \int_{-\infty}^{\infty} f(y) e^{iw(y-nT)} dy \\
&= \sum_{n=0}^N e^{-iwnT} \int_{-\infty}^{\infty} f(y) e^{iwy} dy \\
&= \sum_{n=0}^N e^{-iwnT} \mathcal{F}\{f\}(w) \\
&= \mathcal{F}\{f\}(w) \sum_{n=0}^N e^{-iwnT}
\end{aligned} \tag{3.33}$$

We used the fact that the exponential term  $e^{-iwnT}$  is a constant factor when integrating along  $dy$  and the identity for the Fourier Transform of the function  $f$ . Next, let us examine the series  $\sum_{n=0}^N e^{-iwnT}$  closer:

$$\begin{aligned}
\sum_{n=0}^N e^{-iwnT} &= \sum_{n=0}^N (e^{-iwT})^n \\
&= \frac{1 - e^{iwT(N+1)}}{1 - e^{-iwT}}
\end{aligned} \tag{3.34}$$

We recognize the geometric series identity for the left-hand-side of equation 3.34. Mainly relying on trigonometric identities, equation 3.33 can be further simplified to:

$$\mathcal{F}\{S\}(w) = (p + iq)\mathcal{F}\{f\}(w) \tag{3.35}$$

where  $p$  and  $q$  are defined as:

$$\begin{aligned}
p &= \frac{1}{2} + \frac{1}{2} \left( \frac{\cos(wTN) - \cos(wT(N+1))}{1 - \cos(wT)} \right) \\
q &= \frac{\sin(wT(N+1)) - \sin(wTN) - \sin(wT)}{2(1 - \cos(wT))}
\end{aligned} \tag{3.36}$$

Please notice, all derivation steps can be found in the appendix in section ??.

Now lets consider our actual problem description. Given a patch of a nano-scaled surface snake shed represented as a two dimensional height field  $h(x, y)$ . We once again assume that this provided patch is representing the whole surface  $S$  of our geometry by some number of replicas of itself. Therefore,  $S(x, y) = \sum_{n=0}^N h(x + nT_1, y + mT_2)$ , assuming that the given height field has the dimensions  $T_1$  by  $T_2$ . In order to derive an identity for the two dimensional Fourier transformation of  $S$  we can similarly proceed like we did to derive equation 3.35.

$$\mathcal{F}\{S\}(w_1, w_2) = (p + iq)\mathcal{F}_{DTFT}\{h\}(w_1, w_2) \quad (3.37)$$

Note that a detailed derivation of equation 3.37 can be found in the appendix in section ?? and we have defined :

$$\begin{aligned} p &:= (p_1 p_2 - q_1 q_2) \\ q &:= (p_1 p_2 + q_1 q_2) \end{aligned} \quad (3.38)$$

For the identity of equation 3.37 we made use of Green's integration rule which allowed us to split the double integral to the product of two single integrations. Also, we used the definition of the 2-dimensional inverse Fourier transform of the height field function. We applied a similar substitution like we did in 3.32, but this time twice, once for  $x_1$  and once for  $x_2$  separately. The last step in equation 3.37, substituting with  $p$  and  $q$  in equation ?? will be useful later in the implementation. The insight should be, that the product of two complex numbers is again a complex number. We will have to compute the absolute value of  $\mathcal{F}\{S\}(w_1, w_2)$  which will then be equal  $(p^2 + q^2)^{\frac{1}{2}} |\mathcal{F}\{h\}(w_1, w_2)|$

### 3.6.2 Sinc Interpolation in Frequency Domain

In section 3.6.1 we derived an alternative approach to the gaussian window approach described in section 3.2.3 in order to approximate our height field. We assume that our height field is a superposition of periodically aligned substructures (i.e. finger structures). This so called PQ approach allows us to integrate over one period of a substructure in our height field, instead of iterating over the whole domain. Nevertheless, this main finding, described in equation 3.37, is using the DTFT. Thus, since our original height field is supposed to be a continuous-time band-limited function we can reconstruct it by applying a sinc-interpolation.

In general, for a sinc-interpolation, we are interested in recovering an original analog signal  $x(t)$  from its samples. Therefore, for a given sequence of real numbers  $x[n]$ , representing a digital signal, its correspond continuous function is:

$$x(t) = \sum_{n=-\infty}^{\infty} x[n] \text{sinc}\left(\frac{t - nT}{T}\right) \quad (3.39)$$

which has the Fourier transformation  $X(f)$  whose non-zero values are confined to the region  $|f| \leq \frac{1}{2T} = B$ . When  $x[n]$  represents time samples at interval  $T$  of a continuous function, then the quantity  $f_s = \frac{1}{T}$  is known as its sample rate and  $\frac{f_s}{2}$  denotes the Nyquist frequency. The sampling Theorem states that when a function has a Bandlimit  $B$  less than the Nyquist frequency, then  $x(t)$  is a perfect reconstruction of the original function. Figure 3.6 illustrates a reconstruction of a 1d signal relying on a sinc-interpolation.

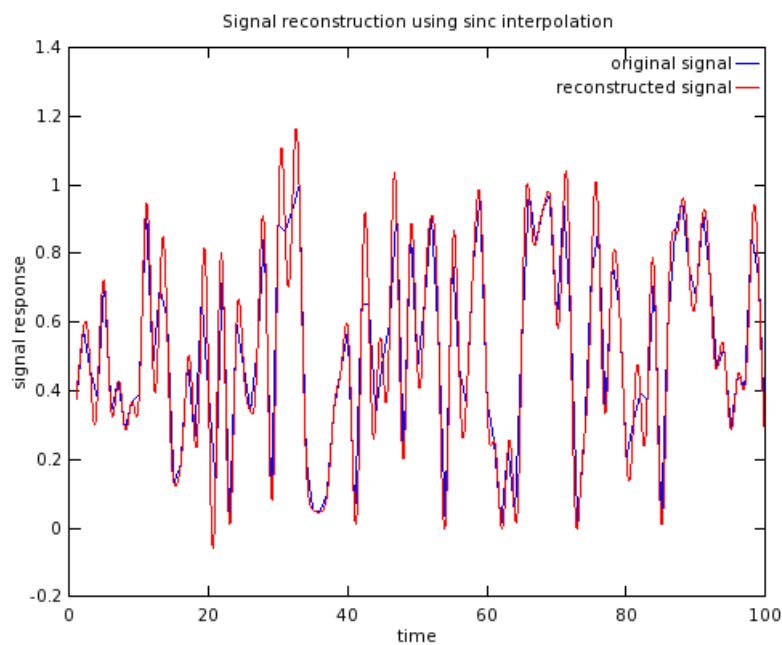


Figure 3.6: Comparison between a given random one dimensional input signal  $s(t)$  and its sinc interpolation  $\hat{s}(t)$ . Notice that for the interpolation there were  $N = 100$  samples from the original signal provided.

# Chapter 4

# Evaluation and Data Acquisition

In this chapter we will provide and discuss an evaluation of our rendering approaches. For this purpose we compare our method's (peak) viewing angles with maximum reflectance for a fixed incident beam with those resulting from the grating equation at different wavelengths. But first we revisit the term diffraction grating and provide a detailed definition.

## 4.1 Diffraction Gratings

In order to evaluate the quality of our simulations, it is important to understand all underlying elements involved in the rendering process. One particular element, which we have not investigated in detail is the diffraction grating represented by our height field. Thus, in this section we will examine in detail, what a diffraction grating actually is and how it works.

By the term *diffraction grating* we are referring to the surface of a flat piece of an opaque material that contains a large number of parallel, closely and evenly spaced slits<sup>1</sup> or bumps. Therefore, these slits are forming a periodically packed, groove-like structure along the surface of the material.

A diffraction grating alters the state of an incident light beam by diffracting its component waves. According to Huygen's principle (see section 2.2.4), when an incident light beam hits the grating points on the slits, the grating will act as point light sources that emits spherical wavelets. Basically, a diffraction grating can be either transmissive (see figure 4.2(*a*)) or reflective (see figure 4.7). As light transmits through or reflects off a grating, the grooves on the grating cause different wavelengths of the light to diffract differently and thus divide the light into its component wavelengths. This also implies that the emitted wave will have a different outgoing angle with peak intensity than the incident light. In general, the closer the spacing of the slits is to the wavelength of the incident wave, the more the emitted wave will be diffracted.

Figure 4.1 illustrates what happens when a monochromatic light passes through a transmissive grating. Using a spectrometer, we see that the outgoing angle of the emitted wave will be different from the incident angle. Hence, the diffracted light is composed of the sum of interfering wave components emanating from each slit in the grating.

---

<sup>1</sup>Usually, these slits are either engraved or etched into the surface of the material.

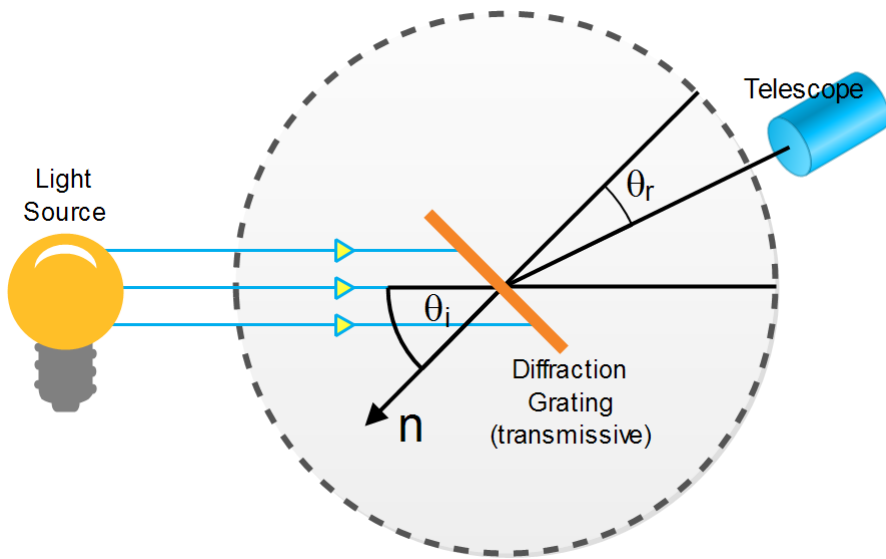


Figure 4.1: Spectrometer: When a beam of monochromatic light passes through a grating placed on a spectrometer, images of the sources can be seen through the telescope at different angles.

Suppose an incident plane wavefront, composed of a monochromatic light source, is directed at a transmissive diffraction grating, parallel to its axis(i.e. its surface normal) as shown in figure 4.2. Let the distance between successive slits on the grating be equal to  $d$ . Furthermore, at a distance  $L$ , there is a screen parallel to the grating. Then the emitted waves will form a diffraction pattern on the screen which is the result of interference effects (constructive or destructive interference) among outgoing wavelets as shown in figure 4.2(a).

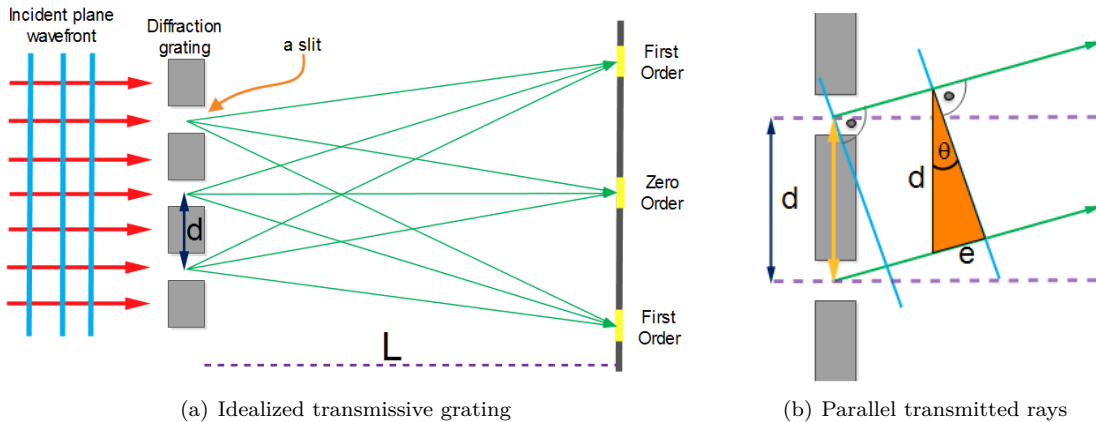


Figure 4.2: Light directed to parallel to grating

If the distance to the screen is much larger than the slits width, i.e.  $L \gg d$ , then all the rays emanating from the surface and ending up at the receiver are parallel. Thus, the path difference between waves from any two adjacent slits can be derived by drawing a perpendicular line between

the parallel rays. Applying simple trigonometry gives us this path difference as  $e = d\sin(\theta)$  as shown in figure 4.2(b). If the path difference equals one wavelength or a multiple of the wave's wavelength, the emerging, reflected waves from all slits will be in phase and a bright line will be observed at that point. Therefore, the condition for a local maxima in the interference pattern is:

$$d\sin(\theta) = m\lambda \quad (4.1)$$

where  $m \in \mathbb{N}_0$  is the order of diffraction and  $\lambda$  is the wavelength. Because  $d$  is very small for a diffraction grating, a beam of monochromatic light passing through it is split into very narrow bright fringes at large angles  $\theta$  (see figure 4.4). Without the loss of generality, either for a transmissive or a reflective diffraction grating type, an analogous derivation for equation 4.1 can be derived.

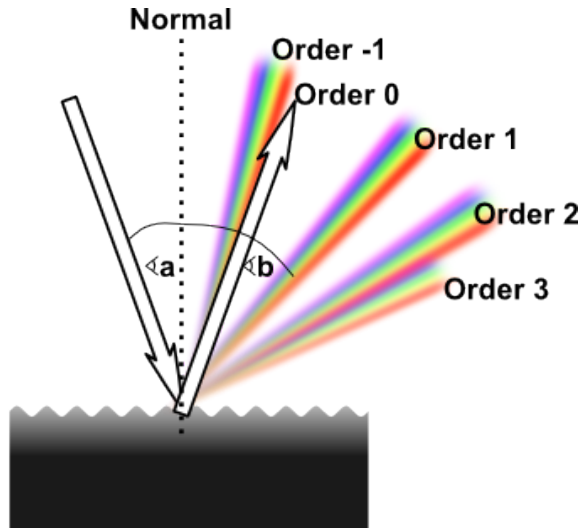


Figure 4.3: Different<sup>2</sup> Orders of diffraction when light is diffracted on a reflective diffraction grating.

When a beam of white light is directed at a diffraction grating along its axis, instead of a monochromatic bright fringe, a set of colored spectra are observed on both sides of the central white band. Figure 4.4 illustrates this for different number of slits on a diffraction grating.

---

<sup>2</sup>This image has been taken from  
[http://www.tau.ac.il/~phchlab/experiments\\_new/SemB01\\_Hydrogen/02TheoreticalBackground.html](http://www.tau.ac.il/~phchlab/experiments_new/SemB01_Hydrogen/02TheoreticalBackground.html)

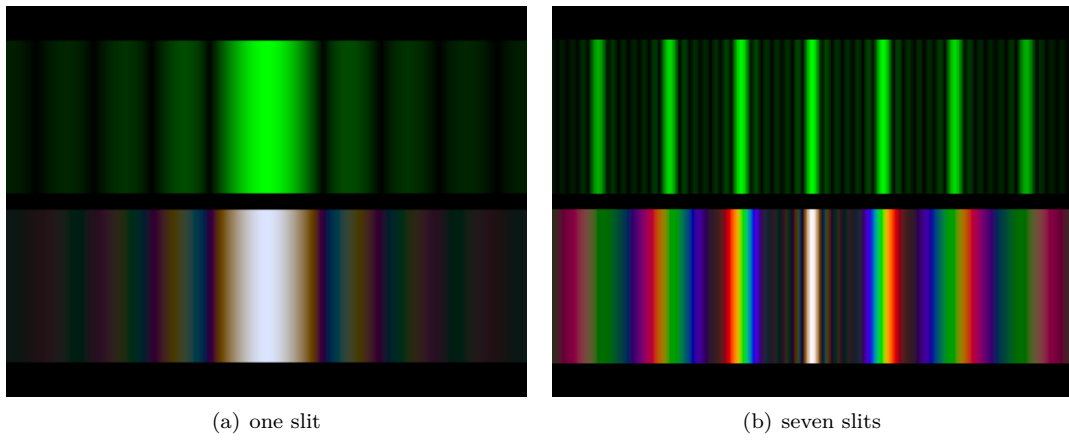


Figure 4.4: Difference of diffraction pattern<sup>3</sup> between a monochromatic (top) and a white (bottom) light spectra for different number of slits.

Since the reflection angle  $\theta_r$  for a maxima increases with wavelength  $\lambda$ , red light, which has the longest wavelength, is diffracted through the largest angle. Similarly violet light has the shortest wavelength and is therefore diffracted the least. Thus, white light is split into its component colors from violet to red light. The spectrum is repeated in the different orders of diffraction, emphasizing certain colors differently, depending on their order of diffraction like shown in figure 4.3. Note that only the zero order spectrum is pure white. Figure 4.5 shows the relative intensity resulting when a beam of light hits a diffraction grating with different number of slits. From the graph we recognise that the more slits a grating has, the sharper more slopes the function of intensity gets. This is similar like saying that, the more periods a grating has, the sharper the diffracted color spectrum gets like shown in figure 4.4.

---

<sup>3</sup>These images have been taken from <http://www.itp.uni-hannover.de/~zawischa/ITP/multibeam.html>

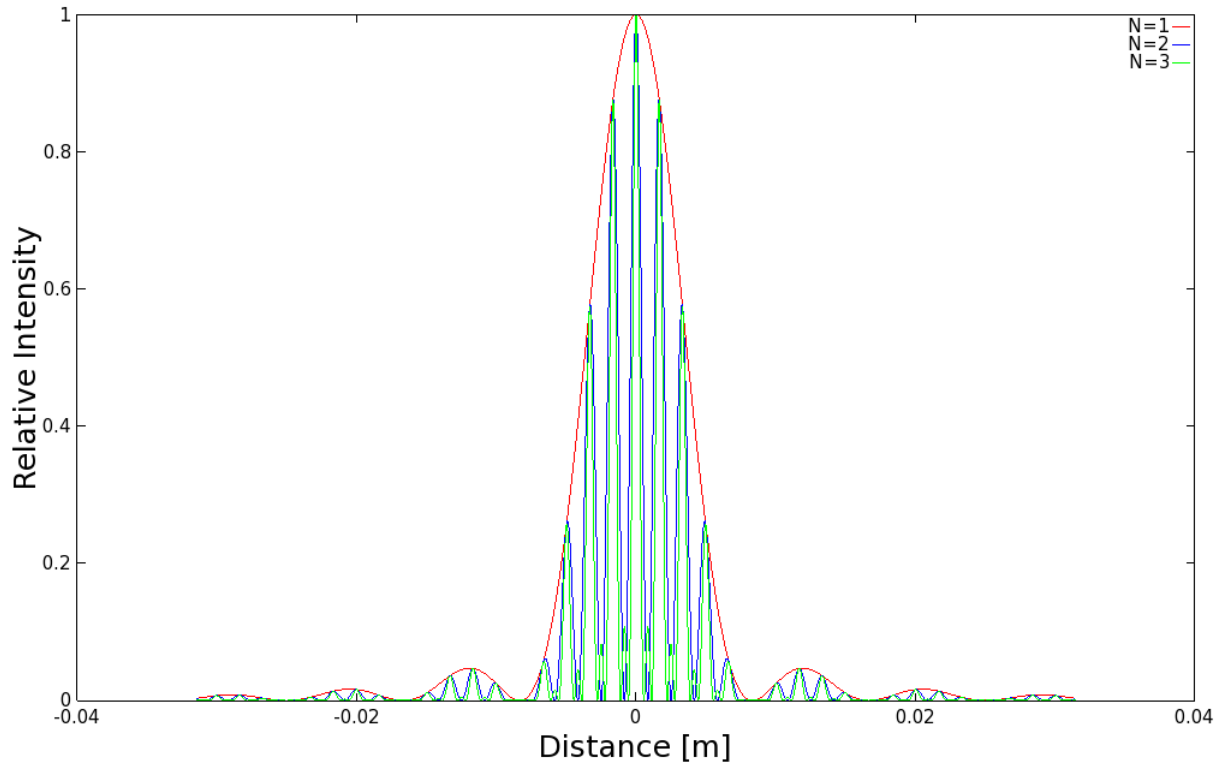


Figure 4.5: Relative intensities of a diffracted beam of light with wavelength  $\lambda = 500\text{nm}$  on a grating for different number of slits  $N$ . A slit width of 30 microns and a slit separation of 0.15 mm was used. The viewer is 0.5m away from the grating.

## 4.2 Data Acquisition

Our goal is to perform physically accurate simulations of diffraction effects due to natural gratings. As for every simulation, its outcome highly depends on the input data and thus we also require measurements<sup>4</sup> of real natural gratings. For that purpose, samples of skin sheds of Xenopeltis and Elaphe snake species were fixed on a glass plate. Then, by using an Atomic Force Microscope (AFM), their surface topography was measured and digitally stored<sup>5</sup>. In general, an AFM is a microscope that uses a tiny probe mounted on a cantilever to scan the surface of an object. The probe is extremely close to the surface, but does not touch it. As the probe traverses the surface, attractive and repulsive forces arising between it and the atoms on the surface inducing forces on the probe that bends the cantilever. The amount of bending is measured and recorded, providing a depth-map of the atoms on the surface. An atomic force microscope is a very high-resolution probe scanner with its demonstrated resolution on the order of a fraction of a nanometer, which is more than 1000 times better than the optical diffraction limit. The resolution of any optical system is limited by the optical diffraction limit due to the effect of diffraction. Thus, no matter how well a lens of an optical system is corrected, its resolution is fundamentally limited by this

<sup>4</sup>All measured data has been provided by the Laboratory of Artificial and Natural Evolution at Geneva - Website:[www.lanevol.org](http://www.lanevol.org)

<sup>5</sup>Note these measured height fields can be visualized using grayscale images, indicating their relative depth.

optical barrier.

### 4.3 Verifications

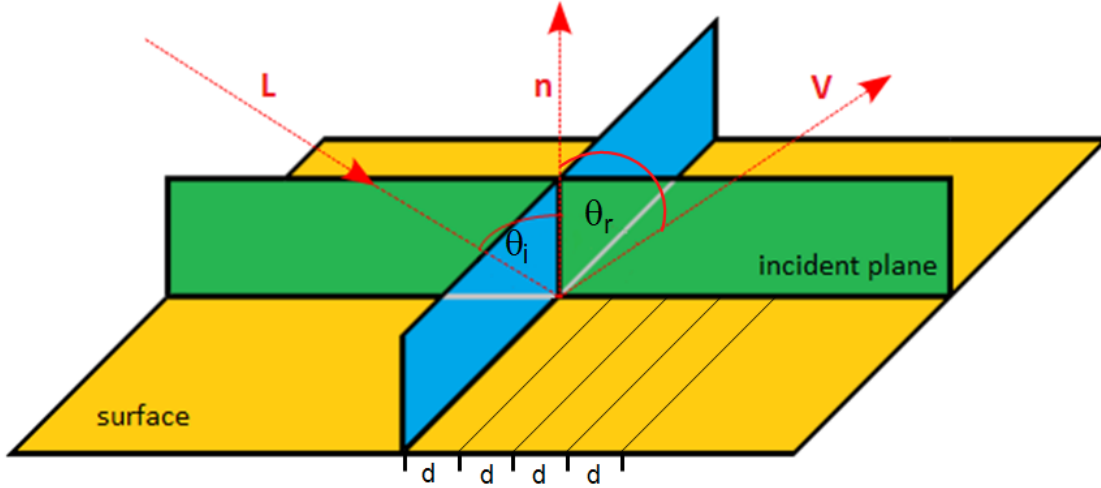


Figure 4.6: Experimental setup for evaluation: A light beam with direction  $L$  hits the surface, representing a grating pattern with periodicity  $d$ , at the incident plane<sup>6</sup> relative to the surface normal  $n$  at angle  $\theta_i$  and emerges at an angle  $\theta_r$  with viewing direction  $V$ .

The physical reliability of our BRDF models has been verified by applying it to a height field for a synthetic blazed grating. Figure 4.6 illustrates the geometrical setup for our evaluation approach: A monochromatic beam of light with wavelength  $\lambda$  hits a surface with periodicity  $d$  at an angle  $\theta_i$  relative to the normal  $n$  along its incident plane. The beam emerges from the surface at the angle  $\theta_r$  with certain intensity as predicted by our model. Note that actually two angles are necessary in order to define a direction vector, using spherical coordinates. However, in our evaluation we fixed the azimuthal angle of these directional vectors (Further information can be found in section 4.3.1).

In our evaluation we compare the local peak angles predicted by our model with those resulting from the grating equation 4.2. The grating equation models the relationship between the grating spacing, the incident light angle and the angle for a local maxima for the diffracted light beam.

---

<sup>6</sup>Remember that in general a direction vector is determined by two angles. In our evaluation setup one angle is initially fixed. Thus, regardless what value we choose for our free angle parameter the incident light will always be parallel to a so called incident plane (green plane shown in figure 4.6).

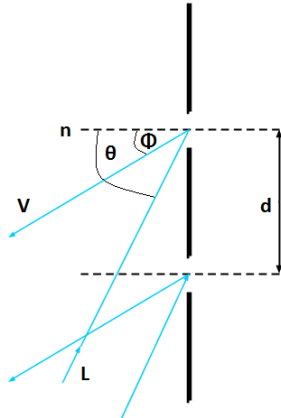


Figure 4.7: Reflecting grating: When the incident light direction is not parallel to its axis at the grating there is another  $\sin(\phi)$  involved. See also the grating equation 4.2.

Figure 4.7 shows that if the incident light is not along the axis of the diffraction gratings then it effects the optical path differences. The angles with locally maximum intensity is given by the grating equation derived from the equation 4.1 following figure 4.7:

$$\sin(\theta_i) = \sin(\theta_r) + \frac{m\lambda}{d} \quad (4.2)$$

In our evaluation we are interested in the first order diffraction, i.e.  $m = 1$ . We further assume that the incident light direction  $L$  is given. In contrast the direction of the reflected wave  $V$  is a free parameter.

In Mathematics, a three dimensional direction vector is fully defined by two angles, i.e. it can be represented by spherical coordinates. Hence,  $\theta_i$ , is a given constant whereas  $\theta_r$  is a free parameter for our evaluation simulation. Therefore, we are going to compare the maxima or the peak viewing angles corresponding to each wavelength using data produced from our method against the maxima resulting by the grating equation 4.2.

### 4.3.1 Numerical Comparisons

In this section we explain how we evaluated the quality of our BRDF models. For a fixed incident light direction we want to compare the peak viewing angles with maximum reflectance for our method with those resulting from the grating equation for different wavelengths. For this purpose we realized the BRDF models corresponding to different gratings for each of our shading approaches, FLSS, NMM and PQ, in Java. By fixing the azimuth angle<sup>7</sup> of the incident light  $L$ - and viewing direction  $V$ , we reduced the degrees of freedom due to these directions, during our evaluation. Thus, any BRDF is then defined by a function that expects as input arguments a wavelength  $\lambda$ , the inclination angle of the incident light  $\theta_i$  - and the viewing direction  $\theta_r$ . The return value of such a function, denoted by  $BRDF(\lambda, \theta_i, \theta_r)$ , is the intensity value of the corresponding BRDF at these given input arguments.

---

<sup>7</sup>Each direction vector in space can be expressed by spherical coordinates. Then, such a unit vector is defined by a pair of two angles, the inclination and the azimuth angle. For further information, please have a look at appendix ??

In our evaluation program we set the incident light angle  $\theta_i$  equal to  $75^\circ$ . This allows us to remove the argument  $\theta_i$  from our BRDF function. Our java program computes each *BRDF* function at a given discrete wavelength-viewing-angle grid, denoted by  $[\Lambda, \Theta]$ . The wavelength space  $\Lambda = [\lambda_{min}, \lambda_{max}]$  and the viewing angle range  $\Theta = [\alpha_{min}, \alpha_{max}]$  of our free parameter  $\theta_r$  are discretized using equidistant steps. The step sizes, denoted by  $(\lambda_{step}, \alpha_{step})$ , are provided as input arguments for our Java evaluation program.

Next, let us have a closer look at how our discrete  $[\Lambda, \Theta]$  grid is constructed. The wavelength space  $\Lambda$ , which is ranging from  $\lambda_{min}$  to  $\lambda_{max}$ , is discretized like the following:

$$\Lambda = \{\lambda = \lambda_{min} + k \cdot \lambda_{step} | k \in \{0, \dots, steps_\lambda - 1\}\} \quad (4.3)$$

where  $steps_\lambda = \lceil \frac{\lambda_{max} - \lambda_{min}}{\lambda_{step}} \rceil$ . We similarly discretise the viewing angle space  $\Theta$  by setting a minimal and maximal viewing-angle boundary  $\alpha_{min}$  and  $\alpha_{max}$ . Then  $\lceil \frac{\alpha_{max} - \alpha_{min}}{\alpha_{step}} \rceil$  is the number of angle  $steps_\alpha$ . And thus, our  $\Theta$  space is defined like the following:

$$\Theta = \{\alpha = \alpha_{min} + k \cdot \alpha_{step} | k \in \{0, \dots, steps_\alpha - 1\}\} \quad (4.4)$$

Then, every BRDF java function is applied to the grid  $[\Lambda, \Theta]$  and the resulting spectral response is stored in a matrix

$$R = \{BRDF(\lambda_i, \theta_r^j) | i \in Index(\Lambda), j \in Index(\Theta)\} \quad (4.5)$$

The generation process of the evaluation plots, which we discuss in section 4.3.2, is described in algorithm 1. This algorithm takes the matrix  $R$  from equation 4.5 as input argument. For the maximal reflectance of our methods at any wavelength, it computes the corresponding peak viewing angles and compares it to the angle resulting from the grating equation.

---

**Algorithm 1** BRDF Evaluation Graph Plotter

---

**Input:**  $R$  Matrix with *BRDF* intensity values of  $(\Lambda, \Theta)$  grid  
 $\Lambda$  discretized wavelength space used to compute  $R$   
 $(\alpha_{min})$  minimum value of viewing angle space  $\Theta$   
 $(\alpha_{step})$  discretization level of viewing angle space  $\Theta$   
 $d$  estimated periodicity of height field  
 $\theta_i$  fixed incident angle

**Procedure:**  $getMaxIntensGridPointsOf(matrix, r)$  : get the column-index of the largest intensity value in the row  $matrix(r, *)$   
 $plotPoint(x, y)$ : draw a point at  $(x, y)$

**Output:** Evaluation Plot of given BRDF model applied on given height field

```

1: Foreach  $\lambda_k \in \Lambda$  do
2:    $\tilde{\alpha} = getMaxIntensGridPointsOf(R, \lambda_k)$                                  $\triangleright \tilde{\alpha} \equiv$  index viewing angle of max. R
3:    $\tilde{\alpha}_{r_k} = \alpha_{min} + \alpha_{step} \cdot \tilde{\alpha}$ 
4:    $\theta_{r_k} = \arcsin \left( \frac{\lambda}{d} - \sin(\theta_i) \right)$                                  $\triangleright$  graph resulting from our BRDF model
5:    $plotPoint(\lambda_k, \tilde{\alpha}_{r_k})$                                                $\triangleright$  graph resulting from grating equation
6:    $plotPoint(\lambda_k, \theta_{r_k})$ 
7: end for

```

---

Algorithm 1 iterates over the wavelength space  $\Lambda$  and generates our evaluation plots. For any wavelength it computes the viewing angle with maximum reflectance and the angle resulting from the grating equation as defined in equation 4.2. Both angles are then plotted for the current wavelength in the current iteration. In the next section we will discuss the generated evaluation plots.

#### 4.3.2 Virtual Testbench

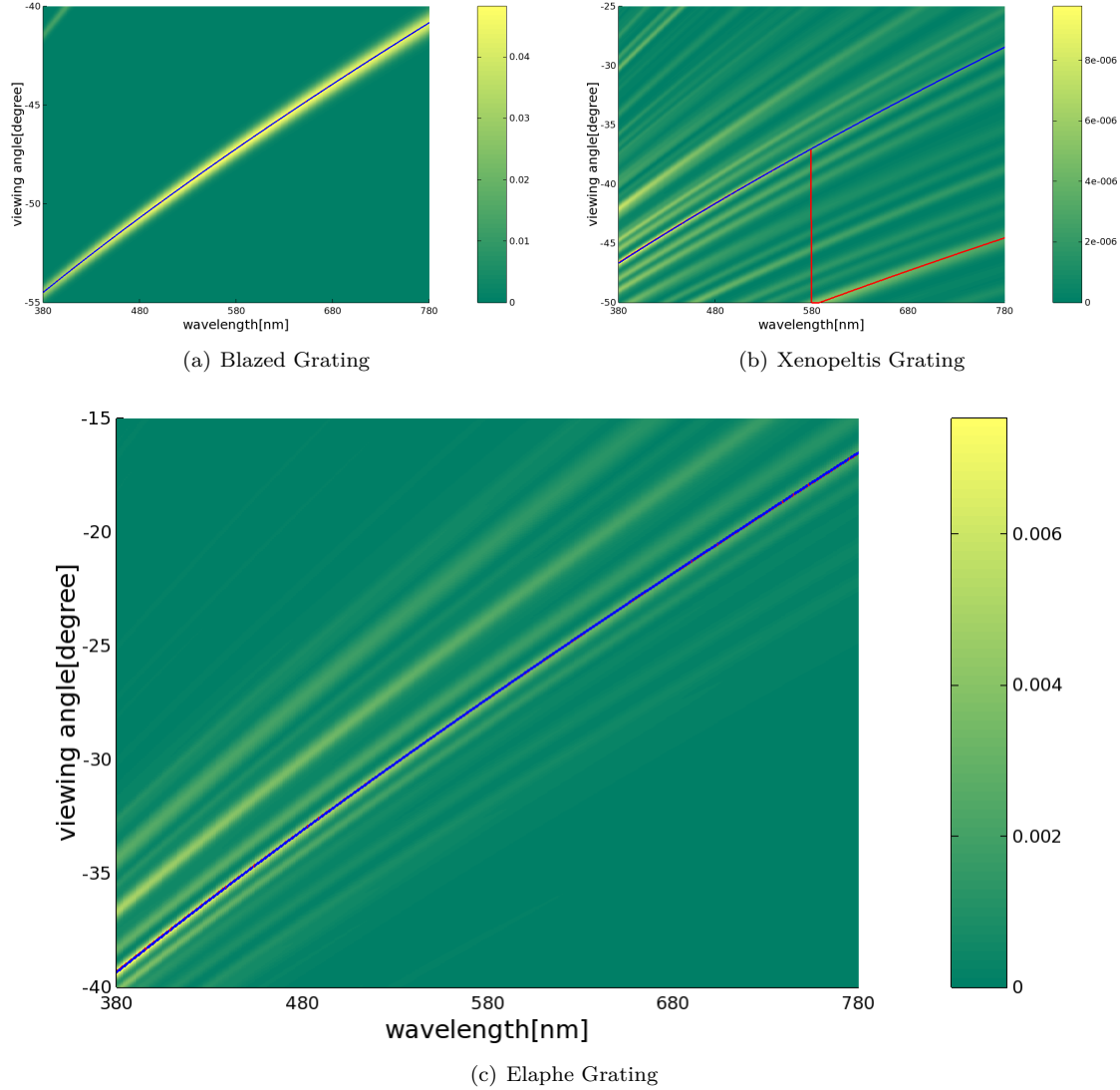


Figure 4.8: Reflectance obtained by using the FLSS approach described in algorithm ??.

In this section we discuss the quality of our BRDF models applied to different surface structures. For that purpose we compare the resulting relative reflectance computed as described in section

4.3.1 for each of our BRDF models to the idealized grating equation 4.2.

|                    | FLSS     |          | NMM      |          | PQ       |          |
|--------------------|----------|----------|----------|----------|----------|----------|
|                    | mean     | variance | mean     | variance | mean     | variance |
| Blazed Grating     | 2499.997 | 0.377    | 2499.997 | 0.377    | 2491.861 | 248.044  |
| Elaphe Grating     | 1144.262 | 0.401    | 1144.179 | 0.677    | 1052.308 | 49.678   |
| Xenopeltis Grating | 1552.27  | 0.45     | -        | -        | -        | -        |

Table 4.1: Statistics of periodicity  $d$  of our used gratings ?? estimated by using the grating equation 4.2.

Figure 4.8 shows the reflectance graphs (BRDF response) resulting from the FLSS approach described in algorithm ?? . This evaluation was applied to an idealized periodic structure, namely to the Blaze- 4.8(a) and to two natural gratings, the Elaphe- 4.8(c) and Xenopeltis grating 4.8(b). For all our evaluation plots, we used an illumination angle of  $\theta_i$  equal to  $75^\circ$ .

Note that higher response values are plotted in yellow and lower values in green. For each of the graphs we determine the viewing angles with peak reflectance for each wavelength and then plot these peak viewing angles versus corresponding wavelengths as solid red curves. The blue curve represents diffraction angles for an idealized periodic structure with a certain periodicity  $d$  according to the grating equation 4.2.

By rearranging the terms of the grating equation defined in equation 4.2 and using the peak reflectance angle  $\alpha_{r_k}$  derived like in algorithm 1 using the matrix  $R$  of equation 4.5, we can compute a periodicity value  $d_k$  for any wavelength  $\lambda_k$ .

$$d_k = \frac{\lambda}{\sin(\alpha_{r_k}) + \sin(\theta_i)} \quad (4.6)$$

By computing the mean value of these  $d_k$  values for all  $\lambda$  in  $\Lambda$  we can compute an estimated periodicity value  $d$ . We estimated these periodicity values for every grating structure and every method we are using. The corresponding periodicity values are tabulated in table 4.1.

The red and blue curve are closely overlapping in our figure 4.8(a) and 4.8(c). For Blaze and Elaphe there is only diffraction along only one direction perceivable. Since the Blazed grating is synthetic we use its exact periodicity to plot the blue curve instead of estimating it. The Xenopeltis grating is evaluated just along the direction for the finger like structures. For Xenopeltis it is interesting to see that the red curve for the peak viewing angle toggles between two ridges corresponding to two different periodicities. This happens because there are multiple sub regions of the nanostructure with slightly different orientations and periodicity. Each sub region carves out a different yellowish ridge. depending on the viewing angle, the reflectance due to one such subregion can be higher than from the others.

Figure 4.9 shows the evaluation plots for the NMM approach applied to the Blazed- (see figure 4.9(b)) and the Elaphe-grating (see figure 4.9(b)). The NMM approach is an optimization of the FLSS approach and is discussed in section ?? . The response curve of each plotted NMM approach graph closely matches the corresponding grating equation curve. Furthermore, the evaluation graphs of the NMM approach look similar to the corresponding evaluation plots of the FLSS approach shown in figure 4.8. Thus, this confirms that the NMM optimization works well.

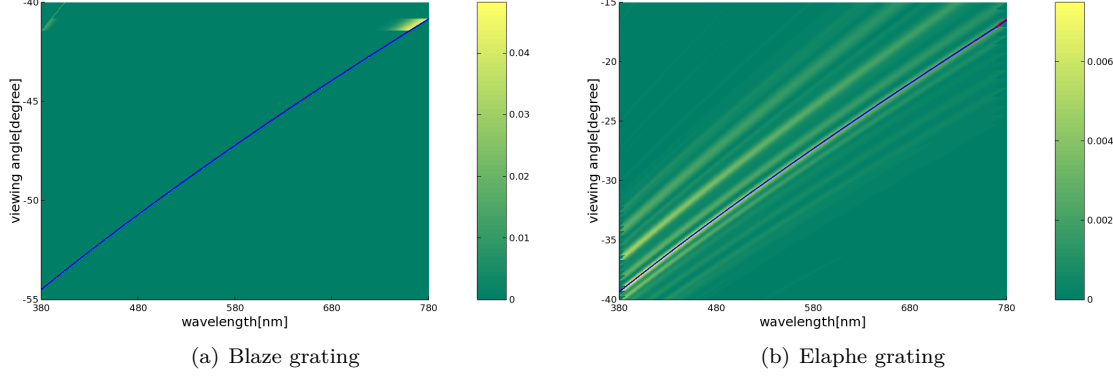


Figure 4.9: Reflectance obtained using NMM optimization approach.

Last, let us consider the evaluation graphs in figure 4.10 for the PQ approach described in algorithm ???. The PQ approach assumes the given grating being periodically distributed on the surface of a shape. For this approach we have plotted evaluation graphs of the Blaze- (See figure 4.10(a)) and Elaphe grating (See figure 4.10(b)). The response curves of both PQ evaluation graphs exhibit some similarities, but also some differences, compared to their corresponding grating equation curves. We could say that the response curve of the blaze grating is weakly oscillating around the grating equation curve (blue), but basically following it even there are some outliers. The response curve of the Elaphe grating is not following its corresponding first order grating equation curve well. This could be due to the PQ's assumption that a given height field has to be periodically distributed along the surface. But in general, for natural gratings, this assumption usually does not hold true. Nevertheless, the red curve fits one of the response curves. We conclude that the PQ approach produces inaccurate results compared to the FLSS approach. Thus, the PQ approach is sub-optimal and unusable in practice.

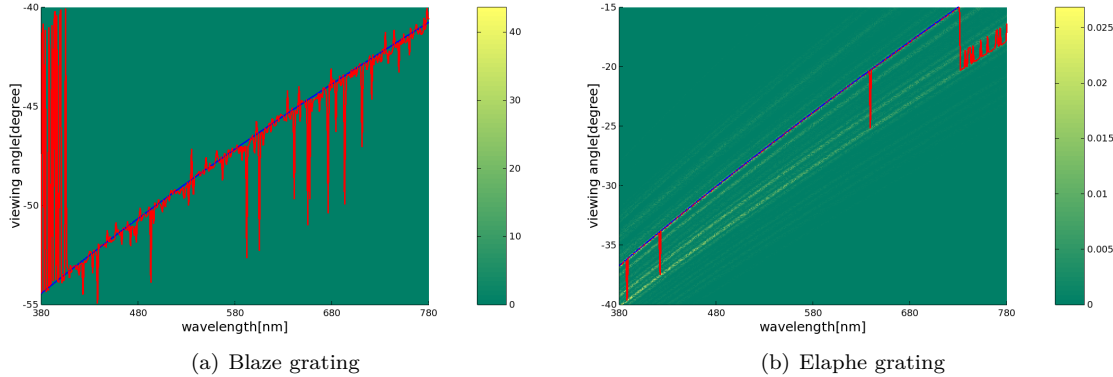


Figure 4.10: Reflectance obtained using PQ optimization approach.

# Bibliography

- [Bar07] BARTSCH, Hans-Jochen: *Taschenbuch Mathematischer Formeln*. 21th edition. HASNER, 2007. – ISBN 978-3-8348-1232-2
- [CT12] CUYPERS T., et a.: Reflectance Model for Diffraction. In: *ACM Trans. Graph.* 31, 5 (2012), September
- [DD14] D.S. DHILLON, et a.: Interactive Diffraction from Biological Nanostructures. In: *EUROGRAPHICS 2014/ M. Paulin and C. Dachsbaucher* (2014), January
- [DM12] DENNIS M, Sullivan: *Quantum Mechanics for Electrical Engineers*. John Wiley Sons, 2012, 2012. – ISBN 978-0470874097
- [D.S14] D.S.DHILLON, M.Single I.Gaponenko M.C. Milinkovitch M. J.Teyssier: Interactive Diffraction from Biological Nanostructures. In: *Submitted at Computer Graphics Forum* (2014)
- [For11] FORSTER, Otto: *Analysis 3*. 6th edition. VIEWEG+TEUBNER, 2011. – ISBN 978-3-8348-1232-2
- [I.N14] I.NEWTON: *Opticks, reprinted*. CreateSpace Independent Publishing Platform, 2014. – ISBN 978-1499151312
- [JG04] JUAN GUARDADO, NVIDIA: Simulating Diffraction. In: *GPU Gems* (2004). <https://developer.nvidia.com/content/gpu-gems-chapter-8-simulating-diffraction>
- [LM95] LEONARD MANDEL, Emil W.: *Optical Coherence and Quantum Optics*. Cambridge University Press, 1995. – ISBN 978-0521417112
- [MT10] MATIN T.R., et a.: Correlating Nanostructures with Function: Structurnal Colors on the Wings of a Malaysian Bee. (2010), August
- [PAT09] PAUL A. TIPLER, Gene M.: *Physik für Wissenschaftler und Ingenieure*. 6th edition. Spektrum Verlag, 2009. – ISBN 978-3-8274-1945-3
- [PS09] P. SHIRLEY, S. M.: *Fundamentals of Computer Graphics*. 3rd edition. A K Peters, Ltd, 2009. – ISBN 978-1-56881-469-8
- [R.H12] R.HOOKE: *Micrographia, reprinted*. CreateSpace Independent Publishing Platform, 2012. – ISBN 978-1470079031
- [RW11] R. WRIGHT, et a.: *OpenGL SuperBible*. 5th edition. Addison-Wesley, 2011. – ISBN 978-0-32-171261-5

- [Sta99] STAM, J.: Diffraction Shaders. In: *SIGGRPAH 99 Conference Proceedings* (1999), August
- [T.Y07] T.YOUNG: *A course of lectures on natural philosophy and the mechanical arts Volume 1 and 2.* Johnson, 1807, 1807